The somatic Golgi nucleates microtubules that are directed by Kinesin-2 to maintain microtubule polarity within neurons

Amrita Mukherjee[1], Paul Brooks[1], Fred Bernard[2], Antoine Guichet[2] and Paul T. Conduit[1,3]

[1]Department of Zoology, University of Cambridge, Downing Street, Cambridge, CB2 3EJ

[2]Université de Paris, CNRS, Institut Jacques Monod, - Bâtiment Buffon, 15 rue Hélène Brion, 75205 Paris CEDEX 13 - France

[3]Corresponding author

Paul Conduit

44-1223-334471

ptc29@cam.ac.uk

Abstract

Neurons contain polarised microtubule arrays essential for neuronal function. Microtubules have fast-growing plus ends and stable minus ends; within axons plus ends grow away from the soma (plus-end-out) and within dendrites they grow towards the soma (minus-end-out). How microtubules are nucleated and how microtubule polarity is established and maintained within neurons remains unclear. We show that within *Drosophila* neurons the major microtubule nucleating complexes, γ-TuRCs, localise to the somatic Golgi, which nucleates microtubules preferentially towards the axon. We find that Kinesin-2, a plus-end-associated motor that "walks" along adjacent microtubules, guides these growing microtubules into axons. In contrast, Kinesin-2 prevents growing microtubules from entering dendrites. We propose that this exclusion occurs when plus-end-associated Kinesin-2 engages with dendritic microtubules of opposite polarity, generating a backward stalling force on the growing plus end. Thus, asymmetric nucleation and Kinesin-2-mediated microtubule guidance contribute to plus-end-out polarity within axons and maintain minus-end-out polarity in dendrites.

Introduction

Microtubules are polarised α/β-tubulin-based polymers essential for cell viability, providing pushing and pulling forces, structural support or tracks for the transport of intracellular cargo (Goodson and Jonasson, 2018). α-tubulin is located at the so-called minus end and β-tubulin is exposed at the so-called plus end, which is typically more dynamic. This inherent microtubule polarity is important for cell polarity, as different motor proteins (Kinesins and Dynein) move cargo along microtubules in a specific direction – Dynein towards the minus end and most Kinesins towards the plus end. In neurons, most plus ends point away from the soma in axons (plus-end-out microtubules), while the microtubules in dendrites are either of mixed polarity or are predominantly minus-end-out (Hill et al., 2012; Kapitein and Hoogenraad, 2015; Kelliher et al., 2019; Tas et al., 2017). This difference between axons and dendrites is important for the correct distribution of cargo throughout the neuron (Harterink et al., 2018; Kapitein and Hoogenraad, 2015; Tas et al., 2017).

Within cells *de novo* assembly of new microtubules, i.e. microtubule nucleation, is kinetically unfavourable and is templated and catalysed by multi-protein γ-tubulin ring complexes (γ-TuRCs) (Tovey and Conduit, 2018). Knockdown of γ-TuRCs within model systems affects dynamic microtubules in all neuronal compartments (Nguyen et al., 2014; Ori-McKenney et al., 2012; Sánchez-Huertas et al., 2016; Yamada and Hayashi, 2019; Yau et al., 2014) and mutations in γ-TuRC genes have been linked to human neurodevelopmental disorders (Bahi-Buisson et al., 2014; Mitani et al., 2019; Poirier et al., 2013). γ-TuRCs are typically inactive until they are recruited to specific sites within cells, such as microtubule organising centres (MTOCs), the cytosol around mitotic chromatin, or the sides of pre-existing microtubules via binding to Augmin/HAUS complexes (Farache et al., 2018; Lin et al., 2014; Meunier and Vernos, 2016; Sanchez and Feldman, 2016; Teixidó-Travesa et al., 2012). A range of MTOCs exist, including centrosomes, the Golgi apparatus and the nuclear envelope, and different cells use different MTOCs to help generate and organise their specific microtubule arrays (Sanchez and Feldman, 2016). γ-TuRC recruitment occurs via γ-TuRC "tethering proteins", such as *Drosophila* Centrosomin (Cnn), that simultaneously

bind to the γ-TuRC and a particular MTOC, and can also help activate the γ-TuRC (Tovey and Conduit, 2018).

Although γ-tubulin is important within neurons (Nguyen et al., 2014; Ori-McKenney et al., 2012; Sánchez-Huertas et al., 2016; Yamada and Hayashi, 2019; Yau et al., 2014), it remains unclear how microtubule nucleation is regulated. During early development of mammalian neurons, the centrosome within the soma nucleates microtubules (Stiess et al., 2010) that are severed and transported into neurites via motor-based microtubule sliding (Baas et al., 2005). Microtubule sliding is also important for axon outgrowth in *Drosophila* cultured neurons (del Castillo et al., 2014; Lu et al., 2013), and for establishing microtubule polarity (del Castillo et al., 2015; Klinman et al., 2017; Rao et al., 2017; Yan et al., 2013; Zheng et al., 2008). Centrosomes are inactivated, however, at later developmental stages (Stiess et al., 2010) and are dispensable for neuronal development in both mammalian and fly neurons (Nguyen et al., 2011; Stiess et al., 2010). No other active MTOCs within the neuronal soma have been described. Nevertheless, microtubules continue to grow within the soma (Nguyen et al., 2011; Sánchez-Huertas et al., 2016), and in mammalian neurons this depends in part on the HAUS complex (Sánchez-Huertas et al., 2016), which is also important for microtubule growth within axons and dendrites (Cunha-Ferreira et al., 2018; Sánchez-Huertas et al., 2016). Some MTOCs have been identified within dendrites: the basal body, or its surrounding region, within the distal part of *C. elegans* ciliated neurons acts as an MTOC, as does a similar region within the URX non-ciliated neuron (Harterink et al., 2018); an MTOC made from endosomes that tracks the dendritic growth cone in *C. elegans* PVD neurons has recently been identified (Liang et al., 2019); and fragments of Golgi called Golgi outposts within the dendrites of *Drosophila* dendritic arborisation (da) are thought to recruit γ-TuRCs and act as MTOCs (Ori-McKenney et al., 2012; Yalgin et al., 2015; Zhou et al., 2014).

Drosophila larval da neurons are a popular *in vivo* neuronal model (Jan and Jan, 2010). Ease of imaging and genetic manipulation coupled with the ability to examine different neuronal classes, each with specific stereotypical dendritic branching patterns, make them a model of choice when examining microtubule organisation

within neurons. Four classes exist, including class I neurons that are proprioceptive and have the simplest “comb-like” dendritic branching pattern, and class IV neurons that are nociceptive and have the most elaborate branching pattern, tiling the surface of the larva (Figure S1) (Grueber et al., 2002). In both neuronal classes, microtubules in axons are predominantly plus-end-out throughout development, but microtubule polarity in dendrites progressively becomes more minus-end-out as the neurons develop; at two days post larval hatching the majority of dynamic microtubules are minus-end-out (Hill et al., 2012; Stone et al., 2008). Microtubule polarity within da neurons can be disrupted under various mutant or RNAi knockdown conditions (Mattie et al., 2010; Nguyen et al., 2014; Ori-McKenney et al., 2012; Rolls and Jegla, 2015; Sears and Broihier, 2016; Weiner et al., 2016; Yalgin et al., 2015; Zhou et al., 2014), but we lack a full understanding of how microtubule polarity is established and maintained.

Golgi outposts are thought to provide localised sites of microtubule nucleation within the dendrites of da neurons to help regulate dendritic outgrowth and microtubule polarity (Ori-McKenney et al., 2012; Yalgin et al., 2015; Zhou et al., 2014). Unlike the somatic Golgi, which comprises cis, medial, and trans compartments organised into stacks and ribbons (Kondylis and Rabouille, 2009; Nakamura et al., 1995), Golgi outposts can be either single- or multi-compartment units with multi-compartment units having a higher propensity to initiate microtubule growth (Zhou et al., 2014). Within class I da neurons, Golgi outpost-mediated nucleation is thought to be dependent on the γ-TuRC-tethering protein Cnn and to help restrict dendritic branching (Yalgin et al., 2015), while within class IV neurons Golgi outpost-mediated nucleation is believed to be dependent on Pericentrin-like protein (Plp) and to help promote dendritic branching (Ori-McKenney et al., 2012). There remains some uncertainty, however, about the role of Golgi outposts in microtubule nucleation, as a separate study that examined the localisation of ectopically expressed γ-tubulin-GFP concluded that γ-tubulin localises predominantly to dendritic branch points in a Golgi outpost-independent manner (Nguyen et al., 2014).

In this study, we initially aimed to identify sites of microtubule nucleation within *Drosophila* da neurons. We used endogenously tagged γ-tubulin-GFP as a proxy for γ-TuRCs and performed a detailed analysis of γ-TuRC localisation within both class I and class IV da neurons. We find variation between neuronal classes in how γ-TuRCs localise within dendrites, but find that the most prominent localisation of γ-TuRCs is at the somatic Golgi within all sensory neurons of the dorsal cluster. This γ-TuRC-Golgi association is not dependent on either Cnn or Plp. Using an *in vivo* microtubule nucleation assay, we show that the somatic Golgi is a genuine site of microtubule nucleation. We find that these Golgi-derived microtubules are preferentially nucleated towards the axon and are then guided into the axon in a Kinesin-2-dependent manner, contributing to axonal plus-end-out microtubule polarity. We also find that Kinesin-2 is responsible for preventing growing microtubules from entering dendrites and thus for maintaining minus-end-out microtubule polarity within proximal dendrites. We propose that plus-end-associated Kinesin-2 guides growing microtubules along a polarised microtubule network and into axons, but generates a stalling force on growing microtubules when they encounter dendritic microtubules of opposite polarity.

Results

A detailed analysis of endogenous γ-tubulin localisation within class I and class IV da neurons

We began by examining the localisation of γ-tubulin (as a proxy for γ-TuRCs) within class I and class IV da neurons. To avoid any potential artefacts induced by ectopic overexpression, we used alleles where γ-tubulin23C (the zygotic form of γ-tubulin) was tagged at its endogenous locus with GFP ((Tovey et al., 2018) and this study). We generated fly stocks expressing two genetic copies of endogenously-tagged γ-tubulin23C-GFP (hereafter γ-tubulin-GFP) and the membrane marker mCD8-RFP, expressed either in class I or class IV da neurons, and imaged living animals. We found that γ-tubulin-GFP was not strongly enriched throughout the dendrites of either neuron (Figure 1A; Figure 2A), but that we could detect discrete accumulations of γ-tubulin-GFP at specific dendritic sites. This varied between class I and class IV neurons, so we describe each neuron in turn below.

For class I da neurons we focussed on the ddaE neuron (hereafter class I neurons), as these have been the most widely characterised. From 13 class I neurons analysed, we detected an average of 1.1 discrete γ-tubulin-GFP puncta per 100μm of dendrite (Figure 1A). Most puncta were just above background intensity levels, although some were bright, and they were more frequently found away from branchpoints (80.2% of puncta) than within branchpoints (19.8% of puncta). We could detect γ-tubulin-GFP signal in 18% of branchpoints; in approximately half of these branchpoints the γ-tubulin-GFP appeared as puncta, often with multiple puncta per branchpoint, while in the other half of branchpoints the γ-tubulin-GFP signal was spread diffusely through the branchpoint (Figure 1B). This diffuse signal was similar to that observed when γ-tubulin-GFP is overexpressed (Nguyen et al., 2014) (Figure S1B), although it appeared that the frequency of branchpoint occupancy and the strength of the endogenous γ-tubulin-GFP signal was lower than that observed with ectopically expressed UAS-γ-tubulin-GFP. We noticed that class I neurons display “bubbles”, where the diameter of the dendrite is locally increased to differing extents (Figure 1A); there were on average 2.6 “bubbles” per 100μm of dendrite with a larger fraction found

further from the soma; ~16.5% of bubbles contained γ-tubulin-GFP signal, either as weak puncta or a diffuse signal (Figure 1C), and ~36.7% of the γ-tubulin-GFP puncta that we observed within dendrites were found within bubbles. To test whether γ-tubulin-GFP puncta within class I dendrites associate with Golgi outposts, we fixed and stained larval preps expressing γ-tubulin-GFP with the neuronal membrane marker HRP and antibodies against GFP and the Golgi protein GM130. Out of 9 neurons from 3 larvae, we could only find one example where γ-tubulin-GFP colocalised with HRP, and in this case GM130 was also colocalised suggesting it was a Golgi outpost (Figure 1D). GM130 labels only multi-compartment Golgi outposts (Zhou et al., 2014) but HRP probably labels most, if not all, Golgi outposts. We chose not to use the ectopically expressed Golgi marker ManII-GFP used in previous studies, as we found that this can form puncta, enrichments, and long stretches within class I dendrites that are not associated with HRP and thus may not represent genuine Golgi outposts, possibly because an excess of ManII protein causes 'leakage' from Golgi compartments (Figure S1C). All γ-tubulin-GFP puncta (except for the single occasion noted above), including those within branchpoints, dendrites and bubbles, did not colocalise with HRP or GM130 (Figure 1E,F). Thus, our data strongly suggests that γ-TuRCs do not typically associate with Golgi outposts within class I neurons, and instead localise to a fraction of branchpoints and dendritic bubbles in a Golgi outpost-independent manner.

For class IV neurons we focussed on the ddaC neuron (hereafter class IV neurons), as these have also been the most widely characterised. We analysed two distinct dendritic regions that we term proximal (within ~100μm of the soma) and distal (over ~200μm from the soma). We detected an average of 2.3 and 0.3 γ-tubulin-GFP puncta per 100μm of dendrite within proximal (10 neurons analysed) and distal (7 neurons analysed) regions, respectively, and the intensity of the majority was only just above background levels, including all of the puncta in the distal regions (Figure 2A). Nevertheless, we consistently observed bright γ-tubulin-GFP puncta within the primary and secondary branchpoints close to the soma (Figure 2A). 44.6% of γ-tubulin-GFP puncta observed in the proximal regions were found within the large primary and secondary branchpoints, and 57% of these branchpoints contained γ-

tubulin-GFP puncta, which were always bright relative to other foci (Figure 2A). Staining with HRP and GM130 antibodies showed that these bright γ-tubulin-GFP puncta associated with Golgi outposts (Figure 2B). Intriguingly, γ-tubulin-GFP only colocalised with HRP puncta that also associated with GM130 (Figure 2B), suggesting that γ-TuRCs are recruited only to multi-compartment Golgi outposts. The high frequency of proximal branchpoints that contained γ-tubulin-GFP puncta contrasted with the near absence of γ-tubulin-GFP puncta within the smaller branchpoints of the distal arbor, where only 1.7% of branchpoints contained detectable but very weak γ-tubulin-GFP signal (Figure 2A insets). In contrast to class I neurons, we found that the vast majority of ectopically expressed ManII-GFP puncta within class IV neurons colocalised with HRP and did not form large accumulations or stretches within the dendrites (Figure 2C), suggesting that ectopically expressed ManII-GFP can be used as a reliable marker of Golgi outposts in class IV neurons. We observed an average of ~12 and ~5 ManII-GFP-positive Golgi outposts per 100μm of dendrite within proximal and distal regions, respectively, which is consistent with previous observations (Zheng et al., 2008) and far higher than the frequency of γ-tubulin-GFP puncta that we observed (compare Figure 2A to Figure 2C). Thus, only Golgi outposts within the proximal branchpoints of class IV neurons appear to associate readily with γ-TuRCs. In contrast to class I neurons, we very rarely observed γ-tubulin-GFP spread diffusely through branchpoints, suggesting that Golgi outpost-independent recruitment of γ-TuRCs to branchpoints is specific to class I neurons. Moreover, we found far fewer dendritic bubbles per 100μm of dendrite in class IV neurons (0.4 and 0.8 per 100μm dendrite in proximal and distal regions, respectively). Collectively, our data show that Golgi outposts within class IV neuron branchpoints close to the soma frequently associate with γ-TuRCs, but that the majority of Golgi outposts do not.

γ-tubulin-GFP localises to the somatic Golgi of sensory neurons in a Cnn- and Plp-independent manner

The most striking and obvious localisation of γ-tubulin-GFP within both class I and class IV neurons was as multiple large bright puncta within their soma (Figure 1A; Figure 2A; Figure 3A-C). We also observed similar puncta within the somas of other nearby sensory neurons (Figure 3A), including external sensory neurons; these

sensory neurons possess basal bodies that appear to associate with large amounts of γ-tubulin-GFP (Figure 3A). Staining with antibodies against HRP and GM130, which in mammals localises to the cis-Golgi, showed that all γ-tubulin-GFP puncta within the soma of all sensory neurons associated with somatic Golgi stacks (Figure 3B,C; Figure S2), which are typically scattered throughout the cytosol in *Drosophila* cells while still maintaining cis-medial-trans polarity (Kondylis and Rabouille, 2009). These Golgi stacks can be oriented either side-on or face-on to the imaging plane, appearing either more elongated or circular, respectively. Our staining showed that the signals of γ-tubulin-GFP and GM130 partially overlapped at side-on stacks, with γ-tubulin-GFP extending further out laterally than GM130 (Figure 3B; Figure S2A); γ-tubulin-GFP surrounded GM130 in a ring-like pattern on face-on stacks (Figure 3C; Figure S2B). Together, this suggests that γ-tubulin-GFP localises on the rims of the cis-Golgi stack.

Two proteins, Cnn and Plp, were possible candidates for γ-TuRC recruitment to the somatic Golgi, as their homologues are required for proper organisation of microtubules at the somatic Golgi in cycling mammalian cells (Rios, 2014; Roubin et al., 2013; Wang et al., 2010; Wu et al., 2016), and Cnn and Plp have been implicated in γ-TuRC recruitment to Golgi outposts in *Drosophila* class I and class IV neurons, respectively (Ori-McKenney et al., 2012; Yalgin et al., 2015). Cnn is a multi-isoform gene with three sets of isoforms driven by three different promoters (Eisman et al., 2009) (Figure S3A). Promoter one drives the best-studied isoform (that we term Cnn-P1) that localises to centrosomes during mitosis; promoter two drives isoforms (Cnn-P2) that are yet to be characterised; and promoter three drives isoforms that are expressed specifically within testes (Chen et al., 2017) and so have not been considered in this study. Immunostaining with antibodies against Cnn revealed very weak, if any, signal within the soma of the sensory neurons and few, if any, obvious puncta within their dendrites; while the presumptive basal bodies of the external sensory neurons displayed a strong Cnn signal (data not shown). Given that antibody staining can be problematic, we generated flies where Cnn-P1 or Cnn-P2 were tagged with GFP at their isoform-specific N-termini (hereafter, GFP-Cnn-P1 and GFP-Cnn-P2; Figure S3A). The GFP insertions appear functional as flies could be kept as homozygous stocks and the localisation of GFP-Cnn-P1 to centrosomes in syncytial

embryos was normal (Movie S1). GFP-Cnn-P1 signal was very weak and inconsistent within the soma of living class I da neurons (Figure 4A). In contrast, we could readily detect clear GFP-Cnn-P1 puncta within distal dendritic bubbles (Figure 4B). In fixed samples, there was a weak GFP-Cnn-P1 signal associated with the somatic Golgi (Figure S3B), although we did not detect GFP-Cnn-P1 associated with HRP puncta within dendrites (Figure S3B; data not shown). We found a strong GFP-Cnn-P1 signal at the presumptive basal bodies of the external sensory neurons (Figure S3B). Collectively our data suggest that GFP-Cnn-P1 does not readily associate with Golgi, but accumulates within a fraction of dendritic bubbles, possibly together with γ-tubulin.

In contrast to GFP-Cnn-P1, we did not detect any obvious GFP-Cnn-P2 signal within the soma or dendrites of da neurons (Figure S3C). Instead, GFP-Cnn-P2 appeared to be expressed within glia cells that ensheath the axons, soma, and part of the proximal dendritic region of the da neurons (Figure S3C). These glia are known to help regulate dendritic development (Han et al., 2011; Sepp and Auld, 2003; Yadav et al., 2019), and thus Cnn-P2 isoforms may have an indirect role in dendritic arbor growth. GFP-Cnn-P2 also localised strongly to the presumptive basal body of external sensory neurons (data not shown). Consistent with the localisation pattern of GFP-Cnn-P1 and GFP-Cnn-P2, γ-tubulin-GFP could still associate with the somatic Golgi in *cnn* mutant larvae, but not to the basal bodies of external sensory neurons (Figure 4C). We therefore conclude that Cnn is dispensable for γ-TuRC recruitment to the somatic Golgi within sensory neurons.

In contrast to Cnn, antibodies against Plp readily stained the somatic Golgi in all sensory neurons, including class I and class IV da neurons (Figure S4A). The Plp signal was, however, offset from the γ-tubulin-GFP signal at Golgi stacks in both class I and class IV da neurons (Figure 5A,B), suggesting that they localise to different Golgi compartments. Plp also associated with the class IV proximal Golgi outposts (Figure 5C) and the presumptive basal bodies of the external sensory neurons (Figure S4B), and was enriched within a fraction of the distal class I dendritic bubbles (Figure S4C). Strikingly, γ-tubulin-GFP localisation at the somatic Golgi of all sensory neurons, including class I and class IV neurons, and at proximal Golgi outposts in class IV

neurons, was unaffected in *plp* mutant larvae, despite the loss of γ-tubulin-GFP at the basal bodies of external sensory cilia (Figure 5D). In summary, neither Plp nor Cnn are required for the efficient recruitment of γ-TuRCs to the somatic Golgi within sensory neurons, or to the few γ-tubulin-GFP positive Golgi outposts within class IV da neurons, but they are required for the localisation of γ-tubulin-GFP to the basal body region within external sensory (es) neurons.

The somatic Golgi within da neurons nucleates microtubules asymmetrically

We next wanted to assess whether the somatic Golgi is an active MTOC. EB1-GFP binds to growing microtubule ends and generates fluorescent "comets" whose origin can represent nucleation sites. We imaged the soma of class I neurons expressing EB1-GFP and the Golgi marker ManII-mCherry and manually tracked each EB1-GFP comet (Figure 6A; Movie S2; the circle of each track represents the latest position of the EB1 comet). Comets could be observed originating both at non-Golgi sites and at Golgi stacks, emerging at different Golgi stacks within the same cell, and emerging sequentially from the same Golgi stack. Intriguingly, many Golgi-derived comets grew towards the axon; measuring the initial angle of each comet's growth relative to the axon entry site (indicated in Figure 6A) showed that there was a strong bias for initial growth towards the axon ($p<0.001$), although some comets did grow away from the axon and thus towards dendrites (Figure 6B).

We also noticed that Golgi-derived comets tended to grow initially in a similar direction to each other, irrespective of their angle from the axon. We therefore generated and plotted normalised resultant vectors (final vector position from a (0,0) origin represented by a blue circle) for the comets from each Golgi stack that produced 2 or more comets (Figure 6C; see Methods). The angle between the positive Y-axis and a line connecting (0,0) and a given circle on the graph is representative of the overall comet angle from the axon; the distance (d) of each circle from (0,0) is representative of the similarity of comet angles (d=1 if all angles are the same; d=0 if all angles are evenly distributed). 77% of the circles were in the upper segments (Figure 6C; $p<0.001$), again showing that there was a preference for comets to emerge towards the axon. Moreover, there was a bias for resultant vector lengths to be large (Figure

6D; $p<0.001$). We conclude that, comets from a particular Golgi stack emerge within a small angle with respect to each other and with a preference towards the axon.

The origin of EB1-GFP comets is not a perfect proxy for microtubule nucleation, as EB1-GFP comets also appear during the regrowth of partially depolymerised microtubules. We therefore performed a microtubule nucleation assay using a temperature-control device (CherryTemp, Cherry Biotech) to cool samples rapidly to 5°C and then re-heat them to 20°C during continuous imaging of the sample. Cooling causes depolymerisation of dynamic microtubules and warming causes their regrowth from their nucleation site; moreover, any comets that appear a significant amount of time after warming represent new nucleation events. We observed no obvious effect on the distribution of the somatic Golgi stacks during cooling-heating cycles (Figure 6E; Movie S3), although thermal-fluctuation-induced movement of the glass coverslip made it difficult to follow the first few timepoints after cooling or warming. When the appropriate focal plane was reached shortly after warming we could observe EB1-GFP comets emerging from the ManII-mCherry-labelled Golgi structures (green-labelled comets, Figure 6E; Movie S3). Moreover, some comets emerged from Golgi stacks relatively late after warming (e.g between 50 and 120s post warming), suggesting that nucleation sites are not all “primed” to nucleate at the same time. Some comets emerged from non-Golgi sites (purple-labelled comets, Figure 6E; Movie S3), suggesting that either other sites of microtubule nucleation exist or that the comets initially grew from Golgi stacks in a different focal plane. Taking the data together, we conclude that the somatic Golgi within *Drosophila* sensory neurons nucleates microtubules asymmetrically towards the axon.

<u>Kinesin-2-dependent plus-end turning and dendritic exclusion maintain microtubule polarity in axons and dendrites</u>

We next wanted to determine the fate of growing microtubules within the soma. We therefore filmed and tracked EB1-GFP comets within the soma and proximal axons and dendrites of nine class I da neurons (Figure 7A; Movie S4). Comets that initiated within the soma often grew into axons, while few entered dendrites; these neurons have a single axon but at least two primary dendrites, but only 7.1% of comets that

initiated within the soma approached the entrance to a dendrite, while 17.9% approached the entrance of the axon (Figure 7C); the remaining 75% of comets terminated within the soma away from the axon or dendrites. Of the 45 comets that approached the entrance to an axon 26 entered (57.8%, which was 10.3% of all comets), while only 4 of the 18 comets (22.2%, 1.6% of all comets) that approached the entrance to a dendrite entered (Figure 7D; $p=0.011$). Moreover, of the 4 comets that entered a dendrite, two appeared to be growing minus ends because they originated from a comet splitting event, where two comets emerge from one and travel in opposite directions (Movie S6). Thus, growing microtubule plus ends within the soma preferentially reach the entrance to the axon and can readily enter, while the few that reach dendrites are normally excluded from entering.

While asymmetric nucleation from the somatic Golgi likely contributes to more microtubule plus ends reaching the axon, we also observed several occasions where microtubules turned towards the axon (Figure 7A; Movie S4). Microtubule turning events have been observed previously within dendritic branchpoints of da neurons, where the microtubules turn towards the soma along stable microtubules (Mattie et al., 2010; Weiner et al., 2016). This depends upon Kinesin-2, which is a heterotrimeric plus-end-directed motor whose regulatory subunit, Kap3, interacts with EB1 via APC (Mattie et al., 2010). It has therefore been proposed that plus-end-associated Kinesin-2 guides growing microtubules along and towards the plus end of adjacent microtubules (Mattie et al., 2010), something that can be recapitulated *in vitro* (Chen et al., 2014; Doodhi et al., 2014). When we depleted Kap3 from class I da neurons by RNAi there was a dramatic reduction in the frequency of microtubule turning events within the soma; of comets that grew for more than 2μm within the soma and that did not traverse the cell cortex, 61.0% displayed turning behaviour in control cells while only 10.4% displayed turning behaviour in Kap3 RNAi cells (Figure 7A,B,E; Movie S4,5; $p<0.001$). Comets in Kap3 RNAi cells tended to change direction only when traversing the edge of the cell or after collision with the nuclear envelope or cell cortex (Figure 7B; Movie S5). As a result, a lower percentage of comets that originated within the soma approached axon entry sites after Kap3 RNAi (Figure 7C; $p<0.001$), although the comets could still readily enter the axons (Figure 7D). Most strikingly, however, a

much higher percentage of comets entered dendrites after Kap3 RNAi: of the 83 comets that approached the entrance to a dendrite 49 entered (59.0%, which is 6.7% of all comets) (Figure 7E; p=0.005)). This led to a dramatic reversal of polarity within proximal primary dendrites (prior to any dendritic branches); in control neurons, the vast majority of comets (135/146; 93.8%) were retrograde (minus-end-out microtubules), while in Kap3 RNAi neurons a large majority (156/229; 68.1%) were anterograde (plus-end-out microtubules) (Figure 7F; $p<0.001$). We therefore conclude that Kinesin-2 is required to guide microtubules growing within the soma towards the axon and to prevent them from entering dendrites, which is essential in order to maintain minus-end-out microtubule polarity within dendrites.

A model for microtubule regulation within the neuronal soma

Based on our observations, and the findings from previous studies (Chen et al., 2014; Doodhi et al., 2014; Mattie et al., 2010; Weiner et al., 2016), we propose a model to explain how microtubules are generated within the soma of da neurons and how microtubule polarity is maintained within their proximal axons and dendrites (Figure 7G). In this model, γ-TuRCs are localised to the cis-Golgi and microtubules are nucleated preferentially towards the axon, generating a polarised microtubule network within the soma. Plus-end-associated Kinesin-2 guides the growing plus ends of the nucleated microtubules along and towards the plus ends of the polarised microtubule network, and thus guides them towards and into the axon. Microtubules that do happen to grow towards a dendrite are excluded from entering when the plus-end-associated Kinesin-2 engages with a dendritic microtubule of opposite polarity and thus exerts a backward stalling force on the growing plus end. Importantly, this model explains how minus-end-out microtubule polarity is maintained within proximal dendrites.

Discussion

We have discovered that Golgi stacks within the soma of *Drosophila* da neurons asymmetrically nucleate microtubules that are guided into the axon and are excluded from entering dendrites in a Kinesin-2-dependent manner. Together with results from previous studies showing that Kinesin-2 binds to plus-tip proteins and can guide the growth of microtubule plus ends (Chen et al., 2014; Doodhi et al., 2014; Mattie et al., 2010; Weiner et al., 2016), our data suggest that plus-end-associated Kinesin-2 guides growing microtubules along an polarised microtubule network into axons, increasing the plus-end-out microtubule pool. In contrast, growing microtubules are excluded from entering dendrites and we propose that this is because plus-end-associated Kinesin-2 exerts a stalling force on these growing microtubules when engaging with dendritic microtubules with opposite polarity. This simple but elegant model explains, for the first time, how minus-end-out microtubule polarity is maintained within proximal dendrites.

Our model can explain how minus-end-out microtubule polarity is maintained, but what is the origin of minus-end-out microtubules? These microtubules could have been pushed from the soma into the dendrites by motor-based sliding. Alternatively, they could have been nucleated at sites within dendrites and then have grown back towards the soma. Retrograde microtubule growth events do occur within the dendrites of da neurons, and some of these growth events originate from Golgi outposts (Ori-McKenney et al., 2012; Yalgin et al., 2015; Zhou et al., 2014). While our data suggest that γ-TuRCs are absent from the majority of Golgi outposts, they are present at a few proximal Golgi outposts within class IV neurons. Moreover, microtubule growth events from Golgi outposts could be independent of γ-TuRCs; other non-γ-TuRC microtubule binding proteins can promote microtubule nucleation *in vitro* (Roostalu and Surrey, 2017), and ectopic Golgi outposts found within the axons of nudE mutants do not appear to promote microtubule growth via γ-TuRCs (Arthur et al., 2015; Yang and Wildonger, 2019). Other types of MTOC may also exist: we have observed accumulations of γ-tubulin at branchpoints and dendritic bubbles in class I neurons; and it was recently shown that an endosome-based MTOC tracks the growing dendritic growth cone within *C. elegans* PVD neurons and nucleates microtubules that

travel back towards the soma (Liang et al., 2019). The authors suggest a similar process may occur in newly developing *Drosophila* class I neurons. Thus, there are several potential mechanisms to generate minus-end-out microtubules within dendrites that should be explored in future.

Microtubule nucleation from the somatic Golgi occurs in cultured mammalian cells (Chabin-Brion et al., 2001; Efimov et al., 2007; Rios, 2014; Rivero et al., 2009; Ríos et al., 2004; Roubin et al., 2013; Wu et al., 2016), where microtubules can also grow in a directional manner to generate polarised microtubule arrays potentially required for fibroblast motility (Efimov et al., 2007) and for cancer cell invasion (Wu et al., 2016). Directed microtubule nucleation likely relies on the inherent polarity of the Golgi stacks. The consensus emerging is that the growing plus ends of microtubules nucleated by γ-TuRCs at the cis-Golgi are stabilised by trans-Golgi-associated plus-tip proteins such as CLASP (Rios, 2014; Sütterlin and Colanzi, 2010; Vinogradova et al., 2009; Zhu and Kaverina, 2013). This would help ensure a cis-to-trans directionality of microtubule growth, but whether this occurs in *Drosophila* neurons remains to be explored.

It was somewhat surprising to find that γ-TuRCs were strongly enriched and that microtubule nucleation occurred at the somatic Golgi within mature neurons. Presumably these microtubules are necessary for neuronal function. It is possible that the microtubule network within the soma and axons needs constant renewal, perhaps because motor-driven cargo transport can damage the microtubule lattice (Triclin et al., 2018). These questions will need to be addressed in future, along with whether the somatic Golgi nucleates microtubules within all *Drosophila* neurons, how γ-TuRCs are recruited to the somatic Golgi, and how asymmetric microtubule nucleation is regulated.

Acknowledgements

This work was supported by a Wellcome Trust and Royal Society Sir Henry Dale Fellowship (105653/Z/14/Z) and an Isaac Newton Trust Research grant (18.23(p)) awarded to PTC, and an Association pour la Recherche sur le Cancer grant (PJA

20181208148) awarded to AG. The work benefited from use of the Imaging Facility, Department of Zoology, supported by Matt Wayland and a Sir Isaac Newton Trust Research Grant (18.07ii(c)).

Author Contributions

PTC and AM designed the study, analysed data and wrote the manuscript. AM performed the vast majority of experiments; PB imaged and quantified ManII-mCherry-labelled Golgi outposts; PTC performed some of the EB1-GFP comet imaging. FB and AG supplied the γ-tubulin-ssss-eGFP fly line.

Declaration of Interests

The authors declare no competing interests.

References

Baas, P.W., Karabay, A., and Qiang, L. (2005). Microtubules cut and run. Trends Cell Biol *15*, 518 524.

Bahi-Buisson, N., Poirier, K., Fourniol, F., Saillour, Y., Valence, S., Lebrun, N., Hully, M., Bianco, C., Boddaert, N., Elie, C., et al. (2014). The wide spectrum of tubulinopathies: what are the key features for the diagnosis? Brain *137*, 1676–1700.

Beaven, R., Dzhindzhev, N.S., Qu, Y., Hahn, I., Dajas-Bailador, F., Ohkura, H., and Prokop, A. (2015). *Drosophila* CLIP-190 and mammalian CLIP-170 display reduced microtubule plus end association in the nervous system. Mol Biol Cell *26*, 1491–1508.

Broadie, K., and Bate, M. (1993). Activity-dependent development of the neuromuscular synapse during *Drosophila* embryogenesis. Neuron *11*, 607–619.

del Castillo, U., Lu, W., Winding, M., Lakonishok, M., and Gelfand, V.I. (2014). Pavarotti/MKLP1 Regulates Microtubule Sliding and Neurite Outgrowth in *Drosophila* Neurons. Curr Biol *25*, 1 6.

del Castillo, U., Winding, M., Lu, W., and Gelfand, V.I. (2015). Interplay between kinesin-1 and cortical dynein during axonal outgrowth and microtubule organization in *Drosophila* neurons. Elife *4*, e10140.

Chabin-Brion, K., Marceiller, J., Perez, F., Settegrana, C., Drechou, A., Durand, G., and Poüs, C. (2001). The Golgi Complex Is a Microtubule-organizing Organelle. Mol Biol Cell *12*, 2047–2060.

Chen, J.V., Buchwalter, R.A., Kao, L.-R., and Megraw, T.L. (2017). A Splice Variant of Centrosomin Converts Mitochondria to Microtubule-Organizing Centers. Curr Biol *27*, 1928 1940.e6.

Chen, Y., Rolls, M.M., and Hancock, W.O. (2014). An EB1-Kinesin Complex Is Sufficient to Steer Microtubule Growth In Vitro. Curr Biol *24*, 316–321.

Conduit, P.T., Feng, Z., Richens, J.H., Baumbach, J., Wainman, A., Bakshi, S.D., Dobbelaere, J., Johnson, S., Lea, S.M., and Raff, J.W. (2014). The centrosome-specific phosphorylation of Cnn by Polo/Plk1 drives Cnn scaffold assembly and centrosome maturation. Dev Cell *28*, 659 669.

Cunha-Ferreira, I., Chazeau, A., Buijs, R.R., Stucchi, R., Will, L., Pan, X., Adolfs, Y., van der Meer, C., Wolthuis, J.C., Kahn, O.I., et al. (2018). The HAUS Complex Is a Key Regulator of Non-centrosomal Microtubule Organization during Neuronal Development. Cell Reports *24*, 791 800.

Dobbelaere, J., Josué, F., Suijkerbuijk, S., Baum, B., Tapon, N., and Raff, J. (2008). A genome-wide RNAi screen to dissect centriole duplication and centrosome maturation in *Drosophila*. Plos Biol *6*, e224.

Doodhi, H., Katrukha, E.A., Kapitein, L.C., and Akhmanova, A. (2014). Mechanical and Geometrical Constraints Control Kinesin-Based Microtubule Guidance. Curr Biol *24*, 322–328.

Efimov, A., Kharitonov, A., Efimova, N., Loncarek, J., Miller, P.M., Andreyeva, N., Gleeson, P., Galjart, N., Maia, A.R., McLeod, I.X., et al. (2007). Asymmetric CLASP-dependent nucleation of noncentrosomal microtubules at the trans-Golgi network. Dev Cell *12*, 917 930.

Eisman, R.C., Phelps, M.A., and Kaufman, T.C. (2009). Centrosomin: a complex mix of long and short isoforms is required for centrosome function during early development in *Drosophila melanogaster*. Genetics *182*, 979 997.

Farache, D., Emorine, L., Haren, L., and Merdes, A. (2018). Assembly and regulation of γ-tubulin complexes. Open Biol *8*, 170266.

Fu, J., and Glover, D.M. (2012). Structured illumination of the interface between centriole and peri-centriolar material. Open Biol *2*, 120104.

Gavilan, M.P., Gandolfo, P., Balestra, F.R., Arias, F., Bornens, M., and Rios, R.M. (2018). The dual role of the centrosome in organizing the microtubule network in interphase. Embo Rep *19*, e45942.

Goodson, H.V., and Jonasson, E.M. (2018). Microtubules and Microtubule-Associated Proteins. Csh Perspect Biol *10*, a022608.

Grueber, W.B., Jan, L.Y., and Jan, Y.-N. (2002). Tiling of the *Drosophila* epidermis by multidendritic sensory neurons. Development (Cambridge, England) *129*, 2867 2878.

Han, C., Jan, L., and Jan, Y.-N. (2011). Enhancer-driven membrane markers for analysis of nonautonomous mechanisms reveal neuron–glia interactions in *Drosophila*. Proc National Acad Sci *108*, 9673–9678.

Harterink, M., Edwards, S.L., de Haan, B., Yau, K., van den Heuvel, S., Kapitein, L.C., Miller, K.G., and Hoogenraad, C.C. (2018). Local microtubule organization promotes cargo transport in C. elegans dendrites. J Cell Sci *131*, jcs.223107.

Hill, S.E., Parmar, M., Gheres, K.W., Guignet, M.A., Huang, Y., Jackson, R.F., and Rolls, M.M. (2012). Development of dendrite polarity in *Drosophila* neurons. Neural Dev *7*, 34.

Hurtado, L., Caballero, C., Gavilan, M.P., Cardenas, J., Bornens, M., and Rios, R.M. (2011). Disconnecting the Golgi ribbon from the centrosome prevents directional cell migration and ciliogenesis. J Cell Biology *193*, 917–933.

Jan, Y.-N., and Jan, L. (2010). Branching out: mechanisms of dendritic arborization.

Nat Rev Neurosci *11*, 316–328.

Kapitein, L.C., and Hoogenraad, C.C. (2015). Building the Neuronal Microtubule Cytoskeleton. Neuron *87*, 492 506.

Kelliher, M.T., Saunders, H.A., and Wildonger, J. (2019). Microtubule control of functional architecture in neurons. Curr Opin Neurobiol *57*, 39–45.

Klinman, E., Tokito, M., and Holzbaur, E.L. (2017). CDK5-dependent activation of dynein in the axon initial segment regulates polarized cargo transport in neurons. Traffic *18*, 808–824.

Kondylis, V., and Rabouille, C. (2009). The Golgi apparatus: Lessons from *Drosophila*. Febs Lett *583*, 3827–3838.

Lee, H., Engel, U., Rusch, J., Scherrer, S., Sheard, K., and Vactor, D. (2004). The Microtubule Plus End Tracking Protein Orbit/MAST/CLASP Acts Downstream of the Tyrosine Kinase Abl in Mediating Axon Guidance. Neuron *42*, 913–926.

Liang, X., Kokes, M., Fetter, R., Pickett, M.A., Sallee, M.D., Moore, A.W., Feldman, J., and Shen, K. (2019). Growth Cone-Localized Microtubule Organizing Center Establishes Microtubule Orientation in Dendrites. Biorxiv 841759.

Lin, T., Neuner, A., and Schiebel, E. (2014). Targeting of γ-tubulin complexes to microtubule organizing centers: conservation and divergence. Trends Cell Biol *25*, 296 307.

Lu, W., Fox, P., Lakonishok, M., Davidson, M.W., and Gelfand, V.I. (2013). Initial neurite outgrowth in *Drosophila* neurons is driven by kinesin-powered microtubule sliding. Curr Biol *23*, 1018 1023.

Lucas, E.P., and Raff, J.W. (2007). Maintaining the proper connection between the

centrioles and the pericentriolar matrix requires *Drosophila* Centrosomin. J Cell Biology *178*, 725–732.

Martinez-Campos, M., Basto, R., Baker, J., Kernan, M., and Raff, J.W. (2004). The *Drosophila* pericentrin-like protein is essential for cilia/flagella function, but appears to be dispensable for mitosis. J Cell Biology *165*, 673–683.

Mattie, F.J., ackpole, M., Stone, M.C., Clippard, J.R., Rudnick, D.A., Qiu, Y., Tao, J., Allender, D.L., Parmar, M., and Rolls, M.M. (2010). Directed microtubule growth, +TIPs, and kinesin-2 are required for uniform microtubule polarity in dendrites. Curr Biol *20*, 2169 2177.

Megraw, T., Li, K., Kao, L., and Kaufman, T. (1999). The centrosomin protein is required for centrosome assembly and function during cleavage in *Drosophila*. Development (Cambridge, England) *126*, 2829 2839.

Mennella, V., Agard, D.A., Huang, B., and Pelletier, L. (2013). Amorphous no more: subdiffraction view of the pericentriolar material architecture. Trends Cell Biol *24*, 188 197.

Meunier, S., and Vernos, I. (2016). Acentrosomal Microtubule Assembly in Mitosis: The Where, When, and How. Trends Cell Biol *26*, 80 87.

Mitani, T., Punetha, J., Akalin, I., Pehlivan, D., Dawidziuk, M., Akdemir, Z., Yilmaz, S., Aslan, E., Hunter, J.V., Hijazi, H., et al. (2019). Bi-allelic Pathogenic Variants in TUBGCP2 Cause Microcephaly and Lissencephaly Spectrum Disorders. Am J Hum Genetics.

Nakamura, N., Rabouille, C., Watson, R., Nilsson, T., Hui, N., Slusarewicz, P., Kreis, T., and Warren, G. (1995). Characterization of a cis-Golgi matrix protein, GM130. J Cell Biology *131*, 1715–1726.

Nguyen, M.M., Stone, M.C., and Rolls, M.M. (2011). Microtubules are organized independently of the centrosome in *Drosophila* neurons. Neural Dev *6*, 38.

Nguyen, M.M., McCracken, C.J., Milner, E., Goetschius, D.J., Weiner, A.T., Long, M.K., Michael, N.L., Munro, S., and Rolls, M.M. (2014). γ-Tubulin controls neuronal microtubule polarity independently of Golgi outposts. Mol Biol Cell *25*, 2039–2050.

Ori-McKenney, K.M., Jan, L., and Jan, Y.-N. (2012). Golgi outposts shape dendrite morphology by functioning as sites of acentrosomal microtubule nucleation in neurons. Neuron *76*, 921 930.

Poirier, K., Lebrun, N., Broix, L., Tian, G., Saillour, Y., Boscheron, C., Parrini, E., Valence, S., Pierre, B., Oger, M., et al. (2013). Mutations in TUBG1, DYNC1H1, KIF5C and KIF2A cause malformations of cortical development and microcephaly. Nat Genet *45*, 639 647.

Rao, A.N., Patil, A., Black, M.M., Craig, E.M., Myers, K.A., Yeung, H.T., and Baas, P.W. (2017). Cytoplasmic Dynein Transports Axonal Microtubules in a Polarity-Sorting Manner. Cell Reports *19*, 2210–2219.

Rios, R. (2014). The centrosome-Golgi apparatus nexus. Philosophical Transactions Royal Soc B Biological Sci *369*, 20130462–20130462.

Rivero, S., Cardenas, J., Bornens, M., and Rios, R.M. (2009). Microtubule nucleation at the cis-side of the Golgi apparatus requires AKAP450 and GM130. Embo J *28*, 1016 1028.

Ríos, R.M., Sanchís, A., Tassin, A., Fedriani, C., and Bornens, M. (2004). GMAP-210 Recruits γ-Tubulin Complexes to cis-Golgi Membranes and Is Required for Golgi Ribbon Formation. Cell *118*, 323–335.

Rolls, M.M., and Jegla, T.J. (2015). Neuronal polarity: an evolutionary perspective. J

Exp Biology *218*, 572–580.

Roostalu, J., and Surrey, T. (2017). Microtubule nucleation: beyond the template. Nat Rev Mol Cell Bio *91*, 321 710.

Roostalu, J., Cade, N.I., and Surrey, T. (2015). Complementary activities of TPX2 and chTOG constitute an efficient importin-regulated microtubule nucleation module. Nat Cell Biol *17*, 1422 1434.

Roubin, R., Acquaviva, C., Chevrier, V., Sedjaï, F., Zyss, D., Birnbaum, D., and Rosnet, O. (2013). Myomegalin is necessary for the formation of centrosomal and Golgi-derived microtubules. Biol Open *2*, 238 250.

Sanchez, A.D., and Feldman, J.L. (2016). Microtubule-organizing centers: from the centrosome to non-centrosomal sites. Curr Opin Cell Biol *44*, 93 101.

Sánchez-Huertas, C., Freixo, F., Viais, R., Lacasa, C., Soriano, E., and Lüders, J. (2016). Non-centrosomal nucleation mediated by augmin organizes microtubules in post-mitotic neurons and controls axonal microtubule polarity. Nat Commun *7*, 12187.

Sears, J.C., and Broihier, H.T. (2016). FoxO regulates microtubule dynamics and polarity to promote dendrite branching in *Drosophila* sensory neurons. Dev Biol *418*, 40 54.

Sepp, K.J., and Auld, V.J. (2003). Reciprocal Interactions between Neurons and Glia Are Required for *Drosophila* Peripheral Nervous System Development. J Neurosci *23*, 8221–8230.

Stiess, M., Maghelli, N., Kapitein, L.C., Gomis-Rüth, S., Wilsch-Bräuninger, M., Hoogenraad, C.C., Tolić-Nørrelykke, I.M., and Bradke, F. (2010). Axon Extension Occurs Independently of Centrosomal Microtubule Nucleation. Science *327*, 704–

707.

Stone, M.C., Roegiers, F., and Rolls, M.M. (2008). Microtubules have opposite orientation in axons and dendrites of *Drosophila* neurons. Mol Biol Cell *19*, 4122 4129.

Stone, M.C., Nguyen, M.M., Tao, J., Allender, D.L., and Rolls, M.M. (2010). Global up-regulation of microtubule dynamics and polarity reversal during regeneration of an axon from a dendrite. Mol Biol Cell *21*, 767 777.

Sütterlin, C., and Colanzi, A. (2010). The Golgi and the centrosome: building a functional partnership. J Cell Biology *188*, 621–628.

Tas, R.P., Chazeau, A., Cloin, B., Lambers, M., Hoogenraad, C.C., and Kapitein, L.C. (2017). Differentiation between Oppositely Oriented Microtubules Controls Polarized Neuronal Transport. Neuron *96*, 1264-1271.e5.

Teixidó-Travesa, N., Roig, J., and Lüders, J. (2012). The where, when and how of microtubule nucleation - one ring to rule them all. J Cell Sci *125*, 4445 4456.

Tovey, C.A., and Conduit, P.T. (2018). Microtubule nucleation by γ-tubulin complexes and beyond. Essays Biochem *91*, EBC20180028.

Tovey, C.A., Tubman, C.E., Hamrud, E., Zhu, Z., Dyas, A.E., Butterfield, A.N., Fyfe, A., Johnson, E., and Conduit, P.T. (2018). γ-TuRC Heterogeneity Revealed by Analysis of Mozart1. Curr Biol *28*, 2314 2323.e6.

Triclin, S., Inoue, D., Gaillard, J., Htet, Z., Santis, M., Portran, D., Derivery, E., Aumeier, C., Schaedel, L., John, K., et al. (2018). Self-repair protects microtubules from their destruction by molecular motors. Biorxiv 499020.

Vinogradova, T., Miller, P.M., and Kaverina, I. (2009). Microtubule network

asymmetry in motile cells: role of Golgi-derived array. Cell Cycle *8*, 2168 2174.

Wang, Z., Wu, T., Shi, L., Zhang, L., Zheng, W., Qu, J.Y., Niu, R., and Qi, R.Z. (2010). Conserved Motif of CDK5RAP2 Mediates Its Localization to Centrosomes and the Golgi Complex. J Biol Chem *285*, 22658–22665.

Weiner, A.T., Lanz, M.C., Goetschius, D.J., Hancock, W.O., and Rolls, M.M. (2016). Kinesin-2 and Apc function at dendrite branch points to resolve microtubule collisions. Cytoskeleton *73*, 35–44.

Woodruff, J.B., Gomes, B., Widlund, P.O., Mahamid, J., Honigmann, A., and Hyman, A.A. (2017). The Centrosome Is a Selective Condensate that Nucleates Microtubules by Concentrating Tubulin. Cell *169*, 1066 1077.e10.

Wu, J., de Heus, C., Liu, Q., Bouchet, B.P., Noordstra, I., Jiang, K., Hua, S., Martin, M., Yang, C., Grigoriev, I., et al. (2016). Molecular Pathway of Microtubule Organization at the Golgi Apparatus. Dev Cell *39*, 44 60.

Yadav, S., Younger, S.H., Zhang, L., Thompson-Peer, K.L., Li, T., Jan, L.Y., and Jan, Y. (2019). Glial ensheathment of the somatodendritic compartment regulates sensory neuron structure and activity. Proc National Acad Sci *116*, 201814456.

Yalgin, C., Ebrahimi, S., Delandre, C., Yoong, L., Akimoto, S., Tran, H., Amikura, R., Spokony, R., Torben-Nielsen, B., White, K.P., et al. (2015). Centrosomin represses dendrite branching by orienting microtubule nucleation. Nat Neurosci *18*, 1437 1445.

Yamada, M., and Hayashi, K. (2019). Microtubule nucleation in the cytoplasm of developing cortical neurons and its regulation by brain-derived neurotrophic factor. Cytoskeleton *76*, 339–345.

Yan, J., Chao, D.L., Toba, S., Koyasako, K., Yasunaga, T., Hirotsune, S., and Shen, K. (2013). Kinesin-1 regulates dendrite microtubule polarity in *Caenorhabditis*

elegans. Elife *2*, e00133.

Yau, K., van Beuningen, S.F., Cunha-Ferreira, I., Cloin, B.M., van Battum, E.Y., Will, L., Schätzle, P., Tas, R.P., van Krugten, J., Katrukha, E.A., et al. (2014). Microtubule Minus-End Binding Protein CAMSAP2 Controls Axon Specification and Dendrite Development. Neuron *82*, 1058 1073.

Zheng, Y., Wildonger, J., Ye, B., Zhang, Y., Kita, A., Younger, S.H., Zimmerman, S., Jan, L., and Jan, Y.-N. (2008). Dynein is required for polarized dendritic transport and uniform microtubule orientation in axons. Nat Cell Biol *10*, 1172 1180.

Zhou, W., Chang, J., Wang, X., Savelieff, M.G., Zhao, Y., Ke, S., and Ye, B. (2014). GM130 is required for compartmental organization of dendritic Golgi outposts. Curr Biol *24*, 1227 1233.

Zhu, X., and Kaverina, I. (2013). Golgi as an MTOC: making microtubules for its own good. Histochem Cell Biol *140*, 361–367.

Zimyanin, V.L., Belaya, K., Pecreaux, J., Gilchrist, M.J., Clark, A., Davis, I., and Johnston, D. (2008). In vivo imaging of *oskar* mRNA transport reveals the mechanism of posterior localization. Cell *134*, 843 853.

Figure legends

Figure 1

Endogenously-tagged γ-tubulin-GFP localises to a fraction of branchpoints and dendritic bubbles within class I da neurons. (**A**) Fluorescent confocal images of the proximal region of a class I da neurons expressing mCD8-RFP (greyscale) within a living 3rd instar larva expressing endogenously-tagged γ-tubulin-GFP (green). Left panel (A) shows an overlay of the GFP and RFP signals, right panel (A') shows only the GFP signal with the outline of the neuron drawn for clarity; white, blue and orange arrowheads indicate γ-tubulin-GFP puncta/accumulations within dendritic stretches, branchpoints, and dendritic bubbles, respectively. (**B,C**) Selected images of γ-tubulin-GFP-positive branchpoints (B) or dendritic bubbles (C) from living neurons as in (A). (**D-F**) Confocal images show branchpoints (D,E) or dendritic bubbles (F) from 3rd instar larvae expressing endogenous γ-tubulin-GFP fixed and immunostained for GFP (green), GM130 (magenta) and HRP (greyscale). γ-tubulin-GFP signal was rarely observed co-localising with GM130 and HRP signal (D), and frequently observed independent of the Golgi markers at both branchpoints (E) and dendritic bubbles (F). See also Figure S1.

Figure 2

Endogenously-tagged γ-tubulin-GFP localises to a small fraction of proximal Golgi outposts within class IV da neurons. (**A**) Fluorescent confocal images of the proximal region of a class IV da neuron expressing UAS-mCD8-RFP (greyscale) within a living 3rd instar larva expressing endogenously-tagged γ-tubulin-GFP (green). Left panel (A) shows an overlay of the GFP and RFP signals, right panel (A') shows only the GFP signal with the outline of the neuron drawn for clarity; insets show examples of distal dendrites located >200μm from the soma; white and yellow arrowheads indicate bright or weak γ-tubulin-GFP puncta, respectively, within proximal or distal dendrites. (**B**) Images show a γ-tubulin-GFP-positive proximal branchpoint from a 3rd instar larva expressing endogenous γ-tubulin-GFP fixed and immunostained for GFP (green), GM130 (magenta) and HRP (greyscale). Asterisks indicate GM130 foci from overlapping epidermal cells. Arrowhead indicates an

example of a γ-tubulin-GFP-positive Golgi outpost observed within proximal class IV branchpoints. (**C**) Confocal images show the proximal region of a class IV dendritic arbor within a 3rd instar larva expressing ManII-GFP (to mark medial Golgi) fixed and immunostained for GFP (fire) and HRP (greyscale within insets). Insets show HRP staining alone. See also Figure S1.

Figure 3

Endogenously-tagged γ-tubulin-GFP localises to the somatic Golgi of sensory neurons. (**A**) Confocal images show the somas and some proximal dendrites of sensory neurons within the dorsal cluster: class I (yellow), class IV (blue), external sensory (pink) and other (orange) from a 3rd instar larva expressing endogenously-tagged γ-tubulin-GFP and immunostained for GFP (green) and HRP (marking Golgi stacks, greyscale). Upper panel (A) shows an overlay of the GFP and HRP signals, lower panel (A') shows only the GFP signal with coloured neuronal outlines drawn for clarity. (**B, C**) Confocal images show the somas of class I (B) or class IV (C) da neurons from a 3rd instar larva expressing endogenously-tagged γ-tubulin-GFP fixed and immunostained for GFP (green), GM130 (magenta) and HRP (greyscale). Enlarged boxes in (B) and (C) show side-on and end-on stacks, respectively. See also Figure S2.

Figure 4

Cnn-P1 is dispensable for γ-tubulin-GFP recruitment to the somatic Golgi. (**A,B**) Fluorescent confocal images of proximal (A) and distal (B) regions of class I da neurons expressing mCD8-RFP (greyscale) within a living 3rd instar larva expressing endogenously-tagged GFP-Cnn-P1 (green). Upper panels show an overlay of the GFP and RFP channels, lower panels show only the GFP channel with the outline of the neurons drawn for clarity. Arrowhead in (A) indicates a rare dendritic GFP-Cnn-P1 puncta within a proximal dendritic bubble, while arrowheads in (B) indicate more frequent GFP-Cnn-P1 accumulations within distal dendritic bubbles. (**C**) Confocal images show the somas and some proximal dendrites of sensory neurons within the dorsal cluster from a 3rd instar *cnn* mutant larva expressing endogenously-tagged γ-tubulin-GFP and immunostained for GFP (green), HRP (greyscale) and Cnn

(magenta). Images in (C') and (C'') show the separate channels for the class I soma and the presumptive basal body of an external sensory neuron, respectively. See also Figure S3.

Figure 5

Endogenous Plp localises to Golgi but is dispensable for γ-tubulin-GFP recruitment. (**A-C**) Confocal images show the somas of a class I (A) or a class IV (B) neuron and a proximal branchpoint of a class IV neuron (C) from 3rd instar larvae expressing γ-tubulin-GFP fixed and immunostained for GFP (green), Plp (magenta) and HRP (greyscale). Arrowhead in (C) indicates a γ-tubulin-GFP-positive Golgi outpost that contains Plp. (**D**) Confocal images show the somas and some proximal dendrites of sensory neurons within the dorsal cluster: class I (yellow), class IV (blue), external sensory (pink) and other (orange), from a *plp* mutant 3rd instar larva expressing endogenously-tagged γ-tubulin-GFP and immunostained for GFP (green), HRP (greyscale) and GM130 (magenta). Left panel (D) shows an overlay of the GFP and HRP signal, with insets showing overlays for different neurons, as indicated; right panel (D') shows the GFP channel with coloured outlines of the different neurons drawn for clarity, with insets showing separate channels for a proximal branchpoint. See also Figure S4.

Figure 6

Somatic Golgi stacks nucleate microtubules. (**A**) Widefield fluorescent images from a movie showing the soma of a class I da neuron expressing EB1-GFP (greyscale) and ManII-mCherry (magenta). Manually assigned multi-colour tracks of EB1-GFP comets were drawn over each image (filled circle = last location of comet). Arrow indicates a Golgi stack from which sequential EB1-GFP comets emerge; dotted lines show an example of an angle measurement of a comet's initial growth relative to the axon entry point (orange circle). Time in min:s from the start of the movie is shown. (**B**) Graph shows a frequency distribution of the initial growth angle (before turning) relative to the axon entry site (as indicated in (A)) of EB1-GFP comets that emerged from Golgi stacks. Negative angles were made positive so as not to distinguish between comets growing to the left or right of the axon. (**C**) Scatter graph shows the

position of the normalised resultant comet vectors (see methods) for each Golgi stack from several neurons. Circle position is representative of the average angle from the axon and how similar the angles were (as indicated). Circle size reflects the number of comets analysed per Golgi stack (as indicated below). (**D**) Graph shows a frequency distribution of the resultant vector lengths for the comet data (blue) and for 3 datasets produced using randomly generated angles (grey shades). (**E**) Widefield fluorescent images from a movie showing the soma of class I da neuron expressing UAS-EB1-GFP (greyscale) and UAS-ManII-mCherry (magenta). The sample was subjected to a warm-cool-warm temperature cycle to induce depolymerisation (5˚C; blue outline) and then repolymerisation (20˚C; red outline) of dynamic microtubules. Tracks were manually colour coded: green = comets emerging from Golgi stacks; purple = comets emerging from elsewhere. Time in min:s from the 5˚C to 20˚C transition is shown. See also Movie S2 and Movie S3.

Figure 7

Microtubules within the soma grow preferentially towards the axon and are excluded from entering dendrites in a Kinesin-2-dependent manner. (**A,B**) Widefield fluorescent images from movies showing the somas of class I da neurons expressing UAS-EB1-GFP and either γ-tubulin-37C RNAi (control) (A) or UAS-Kap3 RNAi (B). Manually assigned multi-colour tracks of EB1-GFP comets are drawn over each image (filled circle = last location of comet). Time in min:s from the start of the movie is shown. (**C**) Graph shows the % of comets that approach either the axon (green) or the dendrites (magenta) in either control or Kinesin-2 RNAi class I da neuron soma, as indicated. (**D**) Graph shows, of the comets that approached, the % of comets that enter the axon (green) or the dendrites (magenta) in either control or Kinesin-2 RNAi class I da neuron soma, as indicated. (**E**) Graph shows the % of applicable comets that display turning events within either control or Kinesin-2 RNAi class I da neuron soma, as indicated. (**F**) Graph shows the % of comets that are anterograde in the proximal primary dendrite (before any branches) in either control or Kinesin-2 RNAi class I da neurons, as indicated. Error bars in (C-F) show the 95% confidence intervals. (**G**) A model depicting microtubule nucleation and growth within the soma of wild type (upper section) or Kinesin-2 depleted (lower section) da neurons. γ-TuRCs

localise to the cis-Golgi and nucleate microtubules preferentially towards the axon (i), creating a polarised microtubule network. In wild type neurons, plus-end-associated Kinesin-2 guides growing microtubules along this network towards the axon (ii). Growing microtubules readily enter axons (iii) but are excluded from entering dendrites (iv), because plus-end-associated Kinesin-2 engages with microtubules of opposite polarity, exerting a backward stalling force on the growing microtubule. In Kinesin-2 depleted neurons, microtubules nucleated from the somatic Golgi grow in straight lines (v) until contact with the nuclear envelope (vi) or the cell cortex (not depicted). Microtubules that approach dendrites can now readily enter (vii) resulting in a loss of overall minus-end-out microtubule polarity.

Materials and methods

Contact for Reagent and Resource Sharing

Further information and requests for resources and reagents should be directed to and will be fulfilled by the Lead Contact, Paul Conduit (ptc29@cam.ac.uk).

Experimental Model and Subject Details

All fly strains were maintained at 18 or 25°C on Iberian fly food made from dry active yeast, agar, and organic pasta flour, supplemented with nipagin, propionic acid, pen/strep and food colouring.

Drosophila melanogaster stocks

The following fluorescent alleles were used in this study: γ-tubulin23C-sfGFP (Tovey et al., 2018), γ-tubulin23c-eGFP (this study), sfGFP-Cnn-P1 (this study), sfGFP-Cnn-P2 (this study), UAS-mCD8-mRFP (BL 27392), UAS-EB1-GFP (BL 35512), UAS-ManII-mCherry (Yuh-Nung Jan), and UAS-ManII-GFP (BL 65248). The following Gal4 lines were used in this study: ppk-Gal4 Chr II (B32078) and Chr III (BL 32079) and 221-Gal4 (BL 26259). The following mutant alleles were used in this study: plp^{5} (BL 9567), plp^{s2172} (BL 12089), cnn^{f04547} (Exelixis at HMS), ppkCD4-tdGFP (BL 35842), KAP RNAi (VDRC 45400 GD), γ-tubulin37C RNAi (BL32513) UAS-Dicer 2 (BL 24646).

For examining the endogenous localisation of γ-tubulin23C we used flies expressing γ-tubulin23C-sfGFP and γ-tubulin23C-eGFP i.e. 2 copies of γ-tubulin23C-GFP, either alone or in combination with one copy of UAS-mCD8-RFP expressed under the control of one copy of either 221-Gal4 or ppk-Gal4. For examining the localisation of Cnn, we used flies expressing two copies of either sfGFP-Cnn-P1 or sfGFP-Cnn-P2 either alone or in combination with one copy of UAS-mCD8-RFP expressed under the control of one copy of either 221-Gal4 or ppk-Gal4. For examining the localisation of Plp in relation to medial Golgi, we used flies with one copy of UAS-ManII-GFP expressed under the control of one copy of either 221-Gal4 or ppk-Gal4. For examining the localisation of γ-tubulin23C in the absence of Cnn or Plp, we used flies expressing two copies of γ-tubulin23C-(sf/e)GFP (as above) in a $cnn^{f04547}/cnn^{f04547}$ or plp^{5}/plp^{s2172}

mutant background. For examining microtubule dynamics in relation to the Golgi we used flies with one copy of UAS-EB1-GFP and one copy of UAS-ManII-mCherry, both expressed under the control of one copy of 221-Gal4. For examining microtubule dynamics in control neurons we used flies with one copy of UAS-EB1-GFP and one copy of UAS-γ-tubulin37C RNAi expressed under the control of one copy of 221-Gal4. For examining microtubule dynamics in Kap3 RNAi neurons we used flies with one copy of UAS-EB1-GFP, one copy of UAS-Dicer 2 and one copy of UAS-Kap3 RNAi expressed under the control of one copy of 221-Gal4.

Method Details

DNA cloning

5-alpha Competent *E. coli* (High Efficiency) (NEB) cells were used for bacterial transformations, DNA fragments were purified using QIAquick Gel Extraction Kits (Qiagen), plasmid purification was performed using QIAprep Spin Miniprep Kits (Qiagen). Phusion High-Fidelity PCR Master Mix with HF Buffer (ThermoFisher Scientific) was used for PCRs.

Generating endogenously-tagged fly lines

All endogenously-tagged lines were made using CRISPR combined with homologous recombination, by combining the presence of a homology-repair vector containing the desired insert with the appropriate guide RNAs and Cas9. The *γ-tubulin23C-eGFP* allele was generated by inDroso by initially inserting an SSSS-eGFP-3'UTR-LoxP-3xP3-dsRED-Lox P cassette before the selection markers were excised. The multi-serine insert acts as a flexible linker between γ-tubulin23C and eGFP. The following guide RNA sequences were used to cut either side of the 3'UTR: AGTCGATCTGTGACCAGCGC and TTATGGTTAATGTCGACTTG. The sfGFP-Cnn-P1 (insertion of sfGFP at the start of exon 1a) and sfGFP-Cnn-P2 (insertion of sfGFP at the start of exon 1b) alleles were generated within the lab following a similar approach to that used previously (Tovey et al., 2018). For GFP-Cnn-P1, flies expressing a single guide RNA (GTCGTGTTTAGACTGGTCCATGGG) were crossed to nos-Cas9 expressing females and the resulting embryos were injected by the Department of Genetics Fly Facility, Cambridge, UK, with a pBluescript plasmid

containing sfGFP and linker sequence (4X GlyGlySer) flanked on either side by 1.5kb of DNA homologous to the *cnn* genomic locus surrounding the 5' end of the appropriate coding region. The homology vectors were made by HiFi assembly (NEB) of PCR fragments generated from genomic DNA prepared from nos-Cas9 flies (using MicroLYSIS, Microzone) and a vector containing the sfGFP tag (DGRC, 1314). For GFP-Cnn-P2 flies, both the guide (GTCGTTAAATGAAACATAGAATA) and the homology vector were injected into nos-Cas9 embryos (BL54591) by Rainbow Transgenic Flies, Inc. Camarillo, CA 93012, USA. F1 and F2 males were screened by PCR using the following primers: for sfGFP-Cnn-P1: forward primer: AAAGTTAACTATTTGAGGACCTCCCATGGTGTCCAAGGGCGAGGAG; reverse primer: CCCGCAAAACCTGTTTAGACTGGTCGGATCCGCCGCTACCTCCGCTTCCACCG GAACCTCCCTTGTACAGCTCATCCATGCC; for sfGFP-Cnn-P2: forward primer: GCAAATGTTAAATGAAAGATACAATATGGTGTCCAAGGGCGAGGAG; reverse primer: GTGAGGTAGATCGAAAGATACCCGCGGATCCGCCGCTACCTCCGCTTCCACCG GAACCTCCCTTGTACAGCTCATCCATGCC.

Antibodies

The following primary antibodies were used: anti-GFP mouse monoclonal at 1:250 (Roche, 11814460001), anti-Cnn Rabbit polyclonal raised against first 660aa of Cnn-P1 (which includes amino acids 35-632 of Cnn-P2) at 1:1000 (Lucas and Raff, 2007), anti-Plp rabbit polyclonal at 1:500 (Martinez-Campos et al., 2004), Alexa-647 conjugated HRP polyclonal at 1:500 (Jackson), and anti-GM130 rabbit polyclonal at 1:300 (Abcam). The following secondary antibodies were used: ATTO-488 GFP-booster at 1:200 (Chromotek), Alexa-488 anti Mouse at 1:500 (ThermoFisher), Alexa-547 anti Rabbit at 1:500 (ThermoFisher).

Immunostaining

Larvae were dissected as described previously (Broadie and Bate, 1993). The fillet preps were fixed in freshly prepared 4% formaldehyde for 20 minutes at room temperature and were then washed four times for 10 minutes in PBST (PBS + 0.1%

TritonX-100). The preps were then blocked in PBST + 5% BSA for 1h at room temperature and incubated with the appropriate primary antibodies diluted in PBST overnight at 4°C. After washing in PBST for ~8h, changing washes every 30-45 minutes, samples were incubated in secondary antibodies diluted in PBST overnight at 4°C. The fillet preps were then washed for ~8h, changing washes every 30-45 minutes in PBST before mounting in Moviol. They were stored at -20°C and imaged within a week.

Fixed and live cell imaging

Imaging of all samples except for those expressing EB1-GFP in neurons or GFP-Cnn-P1 in embryos was carried out on an Olympus FV3000 scanning inverted confocal system run by FV-OSR software using a 60X 1.4NA silicon immersion lens (UPLSAPO60xSiicon). For live samples, wandering L3 larvae were placed in a drop of glycerol and flattened between a slide and a 22X22mm coverslip, held in place by double-sided sticky tape, and imaged immediately. Imaging of EB1-GFP within da neurons and GFP-Cnn-P1 within embryos was performed on a Leica DM IL LED inverted microscope controlled by μManager software and coupled to a RetigaR1 monochrome camera (QImaging) and a CoolLED pE-300 Ultra light source using a 63X 1.3NA oil objective (Leica 11506384). For EB1-GFP imaging, larvae were dissected in live imaging solution (ThermoFisher) to remove the majority of their tissues and mounted in Schneider's media supplemented with FBS and Pen/strep between a slide and 22X22mm coverslip held in place with tape and imaged immediately. When using the CherryTemp, the larvae were held between the CherryTemp chip and a 22X22mm coverslip. The CherryTemp software was used to rapidly change the temperature of the liquid within the flow chamber from 20°C to 5°C after an initial 45s of imaging. The temperature was then rapidly changed back to 20°C after a further 180s and the neurons were imaged for a further 135s. For all EB1-GFP imaging, single Z-plane images were acquired every 3 seconds. All images were processed using Fiji (ImageJ). EB1 comets were tracked using the Manual Tracking plugin in Fiji.

Quantification and Statistical Analysis

Statistical analysis and graph production were performed using GraphPad Prism. For EB1-comet analysis, we excluded comets that were present within the first timepoint (and thus may not represent newly growing microtubules). The angle of initial comet growth was measured using the angle tool within ImageJ, by drawing lines from the axon entry site to the comet origin and then along the initial linear path of the comet. For the frequency distribution of comet angles in Figure 6B, the negative angles (representing comets growing to the left of the axon) were made positive, so as not to distinguish between comets growing to the left and right of the axon, creating a distribution between 0˚ and 180˚. A total of 163 comets from 59 Golgi stacks from 7 cells were analysed.

For the vector analysis in Figure 6C,D we used both positive and negative angles (between -180˚ and 180˚). Initially, a vector for each comet was generated with a length of 1 by calculating cosine(angle) (Y value) and sin(angle) (X value). Taking in turn each Golgi stack that generated more than one comet, the vectors of each comet were added together to generate a resultant vector. These resultant vectors were then normalised by dividing their X and Y values by the number of comets originating from the Golgi stack, such that the maximum length of the resultant vector would be 1, irrespective of comet number. These normalised resultant vectors were plotted as circles on a scatter plot, with the size of each circle reflecting the number of comets originating from that particular Golgi stack. We generated random datasets by replacing each comet angle with a randomly generated number between -180 and 180 to show what results could be expected if the angles of comets originating from Golgi stacks were independent of each other and of the position of the axon. We generated three random datasets, the resultant vector length distributions of which are included in Figure 6D.

One-way Chi-squared tests were used to determine whether frequency distributions were significantly different from the distribution expected by chance i.e. if comet angles were random; a binomial probability calculator was used to determine the chance of observing the skewed distribution between upper (towards the axon) and lower (away from the axon) segments in the resultant vector scatter plot in Figure 6C.

To assess whether comets that originated within the soma approached and entered axons or dendrites, we defined a region (~0.5μm wide) across the entrance to the axon or dendrite; any comets that entered this region were scored as comets that had approached; any comets that crossed this region were scored as comets that entered. For control neurons, we analysed a total of 252 comets from 9 cells (average of 6.29 comets per minute); for Kap3 RNAi we analysed a total of 729 comets from 6 cells (average of 20.3 comets per minute). To assess the polarity of dynamic microtubules within the proximal dendritic regions, we included both comets that originated within the proximal dendrite and those that grew into the dendrite from the soma. For control neurons, we analysed a total of 146 comets from 9 cells; for Kap3 RNAi we analysed a total of 229 comets from 6 cells. The overall proportion of comets that either turned, approached, entered or had anterograde polarity was plotted in Figure 7C-F along with the 95% confidence interval for each dataset. Datasets were compared using one-way Chi-squared tests.

Supplementary Figure legends

Figure S1 – related to Figure 1

Ectopically expressed γ-tubulin-GFP is strongly enriched in branchpoints and dendritic bubbles and ectopically expressed ManII is not a reliable marker of Golgi outposts in class I da neurons. (**A**) A fluorescent confocal image of the anterior region of a 3rd instar larva where mCD8-RFP and mCD4-tdGFP are expressed in class I (magenta) and class IV (green) neurons, respectively. (**A',A''**) Enlarged images of a class I (A') and a class IV (A'') da neuron. (**B**) Fluorescent confocal images of the proximal region of a class I da neuron expressing 221-gal4>UAS-γ-tubulin-GFP (green) and 221-gal4>UAS-ManII-mCherry (magenta) within a living 3rd instar larva. Left panel shows an overlay of the GFP and mCherry channels, middle and right panels show the GFP and mCherry channels, respectively. Blue and orange arrowheads indicate enrichments of ectopically expressed γ-tubulin-GFP within branchpoints and dendritic bubbles, respectively. (**C**) Fluorescent confocal images of distal dendrites from different class I da neurons expressing 221-gal4>UAS-ManII-GFP fixed and immunostained with antibodies against HRP (greyscale). Arrowheads indicate HRP puncta that represent internal membrane, at least some of which could be Golgi outposts. Note that UAS-ManII-GFP spreads into regions of the class I dendrites, including dendritic bubbles, that do not contain HRP puncta, suggesting that over-expressing ManII in class I neurons leads to 'leaking' of the protein outside of Golgi outposts.

Figure S2 – related to Figure 3

Endogenously-tagged γ-tubulin-GFP localises to the somatic Golgi of sensory neurons. (**A,B**) Confocal images show the soma of an external sensory neuron (A) or another sensory neuron within the dorsal cluster (B) from 3rd instar larva expressing two copies of endogenous γ-tubulin-GFP fixed and immunostained with antibodies against GFP (green), GM130 (magenta) and HRP (greyscale). γ-tubulin-GFP and GM130 signals associate at presumptive side-on stacks (extended GM130 signal) and end-on stacks (round GM130 signal) in a way that suggests γ-TuRCs are recruited to the rims of the cis-Golgi.

Figure S3 – related to Figure 4

Cnn-P1 is not strongly associated with the somatic Golgi or Golgi outposts of sensory neurons, while Cnn-P2 is expressed in ensheathing glia. (**A**) A gene diagram of *cnn* to indicate the different Cnn isoforms. Boxed regions are exons, lines are introns. CRISPR combined with homologous recombination was used to insert GFP just after the start codon of either the promoter 1 (P1) or promoter 2 (P2) isoform. Promotor three isoforms are expressed only in testes and so were not analysed in this study. (**B**) Confocal images show the somas and some proximal dendrites of sensory neurons within the dorsal cluster from a 3rd instar larva expressing endogenously-tagged GFP-Cnn-P1 and immunostained with nanobodies against GFP covalently coupled to ATTO-488 (green) and antibodies against HRP (greyscale) and GM130 (magenta). Left panel (B) shows an overlay of the GFP and anti-HRP signals, while the right panel (B') shows the GFP signal with coloured outlines of the different neurons drawn for clarity, with insets showing all channels, including an overlay, for the class I neuron soma, regions of the class IV neuron soma and a class IV proximal branchpoint that contains Golgi outposts. The GFP-Cnn-P1 signal appears very weakly, if at all, at the somatic Golgi and Golgi outposts marked by HRP and GM130 staining. (**C**) Confocal images show class I da neurons from a live 3rd instar larva expressing 221-Gal4>UAS-mCD8-RFP (magenta) and two copies of endogenously tagged GFP-Cnn-P2. Left panel (C) shows an overlay of the GFP and RFP channels, while the right panel (C') shows just the GFP channel. Note that the GFP-Cnn-P2 surrounds the axons and somas of the neurons, suggestive of localisation within ensheathing glia. The * star indicates a region of very bright RFP signal that has bled through into the GFP channel.

Figure S4 – related to Figure 5

Plp localises to the somatic Golgi, Golgi outposts, basal bodies and class I - specific dendritic bubbles.

(**A**) Confocal images show the somas and some proximal dendrites of sensory neurons within the dorsal cluster from a 3rd instar larva expressing ppk-mCD4-tdGFP and immunostained with antibodies against GFP (green), HRP (greyscale) and Plp

(magenta). Left panel (A) shows the GFP and anti-HRP channels, while the right panel (A') shows the anti-Plp channel; insets show an overlay of the anti-Plp and anti-HRP channels. Plp signal colocalises with the HRP staining that marks the multiple well-distributed Golgi stacks within the neuronal soma of each neuron. Plp also localises to some HRP puncta (presumably Golgi outposts) within the proximal branchpoints of class IV neurons. (**B**) Confocal images show parts of the external sensory neurons containing the basal bodies from a 3rd instar larva expressing two copies of endogenously tagged γ-tubulin-GFP and immunostained with antibodies against GFP (green), HRP (greyscale) and Plp (magenta). (**C**) Confocal images show dendritic bubbles of a class I da neuron from a 3rd instar larva immunostained with antibodies against HRP (greyscale) and Plp (magenta).

Supplementary Movie Legends

Movie S1 – related to Figure 4.

Endogenously-tagged GFP-Cnn-P1 localises as expected to centrosomes within *Drosophila* syncytial embryos. The Movie was taken using multi-Z-stack time-lapse epifluorescence microscopy and shows Z-projected images through time of a syncytial embryo expressing endogenously-tagged GFP-Cnn-P1. The cycle starts in M-phase and the centrosomes separate when the cycle transitions to the following S-phase. GFP-Cnn-P1 localises to centrosomes during both M-phase, where the signal is rounded, and S-phase, where the signal displays typical Cnn "flares". Images were collected every 20s and the Movie plays at 20 frames/second.

Movie S2 – related to Figure 6.

EB1-comets emerge from somatic Golgi stacks and initially grow preferentially towards the axon. The Movie was taken using single-Z time-lapse epifluorescence microscopy and shows a class I da neuron expressing 221-Gal4>UAS-EB1-GFP and 221-Gal4>UAS-ManII-mCherry. The left panel shows an overlay of the GFP and mCherry channels, while the right panel shows the same overlay with the ImageJ-generated EB1-GFP comet tracks drawn onto the images. The tracks are multi-coloured, as is default for ImageJ, and the colours have no reference to comet type. Comets can be seen emerging from Golgi stacks and this can occur repeatedly from the same stack (see bottom right stack). Images were collected every 3s and the Movie plays at 10 frames/second.

Movie S3 – related to Figure 6.

The somatic Golgi stacks nucleate microtubules. The Movie was taken using single-Z time-lapse epifluorescence microscopy and shows a class I da neuron expressing 221-Gal4>UAS-EB1-GFP and 221-Gal4>UAS-ManII-mCherry. The sample was subjected to a warming-cooling-warming (20˚C-5˚C-20˚C) cycle, as indicated by the red (20˚C) and blue (5˚C) borders. The left panel shows an overlay of the GFP and mCherry channels, while the right panel shows the same overlay with the ImageJ-generated EB1-GFP comet tracks drawn onto the images. The tracks have been manually post-coloured such that green represent comets emerging from

Golgi stacks and purple represent comets emerging from elsewhere within the soma. Comets can be seen emerging from Golgi stacks before cooling, and then all comets stop during the 3 minute cooling period. After warming, comets can be seen emerging from the Golgi stacks, including comets that emerge >1min after warming. Images were collected every 3s and the Movie plays at 10 frames/second.

Movie S4 – related to Figure 7.

Microtubules turn towards the axon and are excluded from entering dendrites. The Movie was taken using single-Z time-lapse epifluorescence microscopy and shows a control class I da neuron expressing 221-Gal4>UAS-EB1-GFP and 221-Gal4>UAS-γ-tubulin-37c-RNAi. The left panel shows the GFP channel, while the right panel shows the GFP channel with the ImageJ-generated EB1-GFP comet tracks drawn onto the images. The tracks are multi-coloured, as is default for ImageJ, and the colours have no reference to comet type. Comets display turning events, indicating that the growing plus ends of microtubules can be guided along pre-existing microtubules. Comets that approach the axon frequently enter and grow down the axon; In contrast, comets that approach a dendrite entry site do not enter (quantified in Figure 7). Images were collected every 5s and the Movie plays at 10 frames/second.

Movie S5 – related to Figure 7.

Kinesin-2 is required for growing microtubules to turn within the soma and to be excluded from entering dendrites. The Movie was taken using single-Z time-lapse epifluorescence microscopy and shows a Kinesin-2 RNAi class I da neuron expressing 221-Gal4>UAS-EB1-GFP and 221-Gal4>UAS-Kap3-RNAi. The left panel shows the GFP channel, while the right panel shows the GFP channel with the ImageJ-generated EB1-GFP comet tracks drawn onto the images. The tracks are multi-coloured, as is default for ImageJ, and the colours have no reference to comet type. Comets can be seen emerging from multiple locations within the soma but unlike in control neurons they do not turn unless they encounter the nuclear envelope or cell cortex, suggesting that Kinesin-2 is required to guide growing microtubules towards the axon. Comets that approach the axon still frequently enter and grow down the axon, and, in contrast to control neurons, comets that approach dendrites also readily

enter (quantified in Figure 7). This shows that Kinesin-2 is also required for excluding growing microtubules from entering dendrites. Images were collected every 5s and the Movie plays at 10 frames/second.

Movie S6 – related to Figure 7.

Growing microtubule minus ends appear to enter dendrites. The Movie was taken using single-Z time-lapse epifluorescence microscopy and shows a class I da neuron expressing 221-Gal4>UAS-EB1-GFP and 221-Gal4>UAS-γ-tubulin37C-RNAi. The left panel shows the GFP channel, while the right panel shows the GFP channel with the ImageJ-generated EB1-GFP comet tracks drawn onto the images. The tracks are multi-coloured, as is default for ImageJ, and the colours have no reference to comet type. Arrowheads in the left panel indicate what appears to be a comet splitting event, suggestive of a microtubule simultaneously growing at both its plus and minus end. The green arrowhead marks the comet that grows into a dendrite. This comet moves slightly slower than the comet marked by the blue arrowhead, indicating that it is the minus end. Another comet, which does not appear from a splitting event, also grows into a dendrite (pink comet – from 01:18 to 02:30); this may therefore be one of the rare plus ends that enters a dendrite. Images were collected every 5s and the Movie plays at 10 frames/second.

KEY RESOURCES TABLE

REAGENT or RESOURCE	SOURCE	IDENTIFIER
Antibodies		
anti-GFP (mouse monoclonal)	Roche	Cat# 11814460001, RRID:AB_390913
anti-Plp	Gift from Jordan Raff	N/A
anti-GM130 (rabbit polyclonal)	Abcam	Cat# ab30637, RRID:AB_732675
anti-Cnn	Gift from Jordan Raff	
HRP-647 conjugate	Gift from Caroline Fabre	Jackson ImmunoResearch 123-605-021 AB_2338967
Mouse Alexa Fluor 488 secondary	Abcam	Cat# ab150117, RRID:AB_2688012
Rabbit Alexa Fluor 568 secondary	ThermoFisher	Cat# A-11036, RRID:AB_10563566
Bacterial and Virus Strains		
Biological Samples		
Chemicals, Peptides, and Recombinant Proteins		
MicroLYSIS Microzone	Clent Life Science	2MLP-250
Critical Commercial Assays		
Mini prep kit	Qiagen	Cat#27106
Gel extraction kit	Qiagen	Cat#28704
Phusion master mix with HF buffer	NEB	Cat#F531
5-alpha competent *E. coli* (High Efficiency)	NEB	Cat#C2987I
HiFi mastermix	NEB	Cat#E2621
Deposited Data		
Experimental Models: Cell Lines		
Experimental Models: Organisms/Strains		
D. melanogaster: w^{1118}	Bloomington Drosophila Stock Center	BDSC: 3605; Flybase: FBgn0003996
D. melanogaster: cnn^{f04547}	Exelixis at Harvard Medical School	Exelixis: f04547; Flybase: FBst1019233
D. melanogaster: plp^{5}	Bloomington Drosophila Stock Center	BDSC: 9567; Flybase: FBst0009567
D. melanogaster: plp^{s2172}	Bloomington Drosophila Stock Center	BDSC: 12089; Flybase: FBst0012089
D. melanogaster: w[*]; P{w[+mC]=UAS-mCD8.ChRFP}3	Bloomington Drosophila Stock Center	BDSC: 27392; Flybase:FBti0115769
D. melanogaster: w[*]; P{w[+mC]=UAS-EB1-GFP}3	Bloomington Drosophila Stock Center	BDSC: 35512; Flybase:FBti0141213
D. melanogaster: w[1118]; P{w[+mC]=UAS-ManII-EGFP}2; TM2/TM6B, Tb[1]	Bloomington Drosophila Stock Center	BDSC: 65248; Flybase: FBti0183675
D. melanogaster: w[1118]; P{w[+mC]=UAS-ManII-mCherry}/CyO	Gift from Yuh-Nung Jan	N/A

D. melanogaster: w[*]; P{w[+mC]=ppk-GAL4.G}2	Bloomington Drosophila Stock Center	BDSC: 32078; Flybase:FBti0127690
D. melanogaster: w[*]; P{w[+mC]=ppk-GAL4.G}3	Bloomington Drosophila Stock Center	BDSC: 32079; Flybase: FBti0131208
D. melanogaster: w[*]; Pin[1]/CyO; P{GawB}221w-	Bloomington Drosophila Stock Center	BDSC: 26259 Flybase: FBti0114336
D. melanogaster: w[1118]; P{w[+mC]=ppk-CD4-tdGFP}1b	Bloomington Drosophila Stock Center	BDSC: 35842 Flybase: FBti0143429
D. melanogaster: P{w[+mC]=UAS-Dcr-2.D}1, w[1118]	Bloomington Drosophila Stock Center	BDSC: 24646 Flybase: FBti0101430
D. melanogaster: y[1] sc[*] v[1] sev[21]; P{y[+t7.7] v[+t1.8]=TRiP.HMS00517}attP2	Bloomington Drosophila Stock Center	BDSC: 32513 Flybase: FBti0132207
D. melanogaster: w1118; P{GD7377}v45400	Vienna Drosophila Resource Centre	VDRC: 45400GD Flybase: FBst0466097
D. melanogaster: sfGFP-cnnP1	This study	N/A
D. melanogaster: sfGFP-cnnP2	This study	N/A
D. melanogaster: gTub23C-sfGFP	Tovey et al., 2018	N/A
D. melanogaster: gTub23C-eGFP	This study	N/A
Oligonucleotides (see table S1 for additional oligos)		
Guide RNA for GFP-Cnn-P1: GTCGTGTTTAGACTGGTCCATGGG	This study	N/A
Guide RNA for GFP-Cnn-P2: GTCGTTAAATGAAACATAGAATA	This study	N/A
Screening for GFP-Cnn-P1: AAAGTTAACTATTTGAGGACCTCCCATG GTGTCCAAGGGCGAGGAG	This study	N/A
Screening for GFP-Cnn-P1: CCCGCAAAACCTGTTTAGACTGGTCGGA TCCGCCGCTACCTCCGCTTCCACCGGA ACCTCCCTTGTACAGCTCATCCATGCC	This study	N/A
Screening for GFP-Cnn-P2: GCAAATGTTAAATGAAAGATACAATATG GTGTCCAAGGGCGAGGAG	This study	N/A
Screening for GFP-Cnn-P2: GTGAGGTAGATCGAAAGATACCCGCGG ATCCGCCGCTACCTCCGCTTCCACCGG AACCTCCCTTGTACAGCTCATCCATGCC	This study	N/A
Recombinant DNA		
pCFD3	Gift from S. Bullock	Addgene 49410
pBS-KS-attB1-2-PT-SA-SD-2-sfGFP-FIAsh-StrepII-TEV-3x-FLAG	DGRC	1314
pBluescript SK+	Gift from S. Bullock	N/A
Software and Algorithms		
Fiji (ImageJ)	Open source	N/A
Snap Gene	Snap Gene	N/A
Prism	Graphpad	N/A
Other		
Voltelef oil 10S	VWR	24627.188

Additional oligo information:

Oligonucleotides	Source	Identifier
Amplifying for Cnn-P1: GAAAGCTAAGCAGATTCTTCAGC	This study	N/A
Amplifying for Cnn-P1: GGGAGGTCCTCAAATAGTTAAC	This study	N/A
Amplifying for Cnn-P1: GACCAGTCTAAACAGGTTTTGC	This study	N/A
Amplifying for Cnn-P1: GCTCTCTGCACGTCCAAATAAAC	This study	N/A
Amplifying for Cnn-P2: CACTCGCTATAGTCTCGATCC	This study	N/A
Amplifying for Cnn-P2: ATTGTATCTTTCATTTAACATTTGCGCTC	This study	N/A
Amplifying for Cnn-P2: GCGGGTATCTTTCGATCTACC	This study	N/A
Amplifying for Cnn-P2: TCCCGTGGAACAGGAACCAC	This study	N/A
Amplifying for GFP-Cnn-P1: AAAGTTAACTATTTGAGGACCTCCCATGGTGTCCAAGGGCGAGGAG	This study	N/A
Amplifying for GFP-Cnn-P1: CCCGCAAAACCTGTTTAGACTGGTCGGATCCGCCGCTACCTCCGCTTC CACCGGAACCTCCCTTGTACAGCTCATCCATGCC	This study	N/A
Amplifying for GFP-Cnn-P2: GCAAATGTTAAATGAAAGATACAATATGGTGTCCAAGGGCGAGGAG	This study	N/A
Amplifying for GFP-Cnn-P2: GTGAGGTAGATCGAAAGATACCCGCGGATCCGCCGCTACCTCCGCTT CCACCGGAACCTCCCTTGTACAGCTCATCCATGCC	This study	N/A
Amplifying pBS for GFP-Cnn-P1: CGGTTTATTTGGACGTGCAGAGAGCGGGGGATCCACTAGTTCTAGAG	This study	N/A
Amplifying pBS for GFP-Cnn-P1: AAGCTGAAGAATCTGCTTAGCTTTCGGGCTGCAGGAATTCGATATC	This study	N/A
Amplifying pBS for GFP-Cnn-P2: TTGCTGTGGTTCCTGTTCCACGGGAGGGGGATCCACTAGTTCTAGAG	This study	N/A
Amplifying pBS for GFP-Cnn-P2: AAGTGGATCGAGACTATAGCGAGTGGGGCTGCAGGAATTCGATATC	This study	N/A

Figure 1

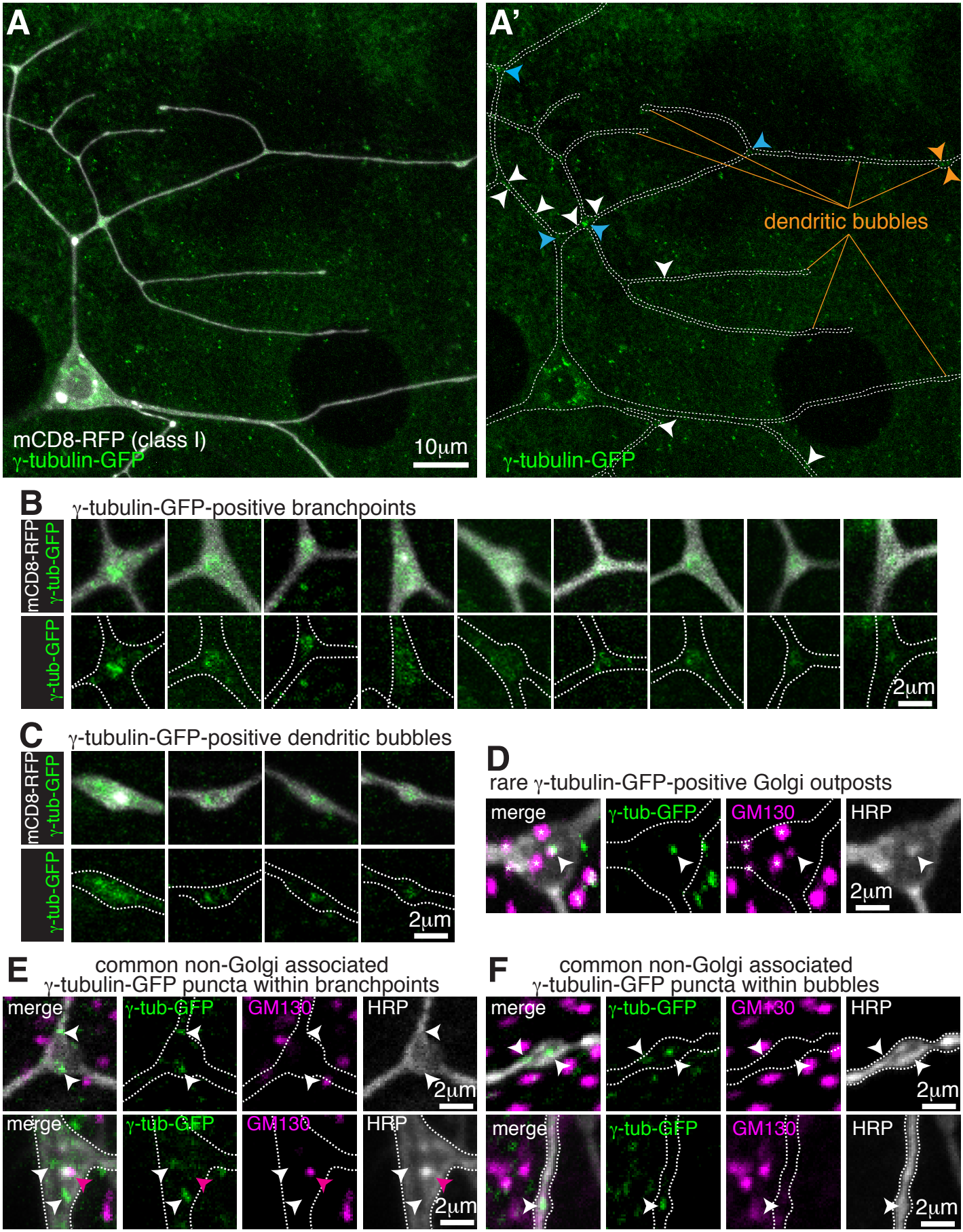
A
mCD8-RFP (class I)
γ-tubulin-GFP
10μm
A'
dendritic bubbles
γ-tubulin-GFP
B
γ-tubulin-GFP-positive branchpoints
mCD8-RFP γ-tub-GFP
γ-tub-GFP
2μm
C
γ-tubulin-GFP-positive dendritic bubbles
mCD8-RFP γ-tub-GFP
γ-tub-GFP
2μm
D
rare γ-tubulin-GFP-positive Golgi outposts
merge
γ-tub-GFP
GM130
HRP
2μm
E
common non-Golgi associated
γ-tubulin-GFP puncta within branchpoints
merge
γ-tub-GFP
GM130
HRP
2μm
F
common non-Golgi associated
γ-tubulin-GFP puncta within bubbles
merge
γ-tub-GFP
GM130
HRP
2μm

Figure 2

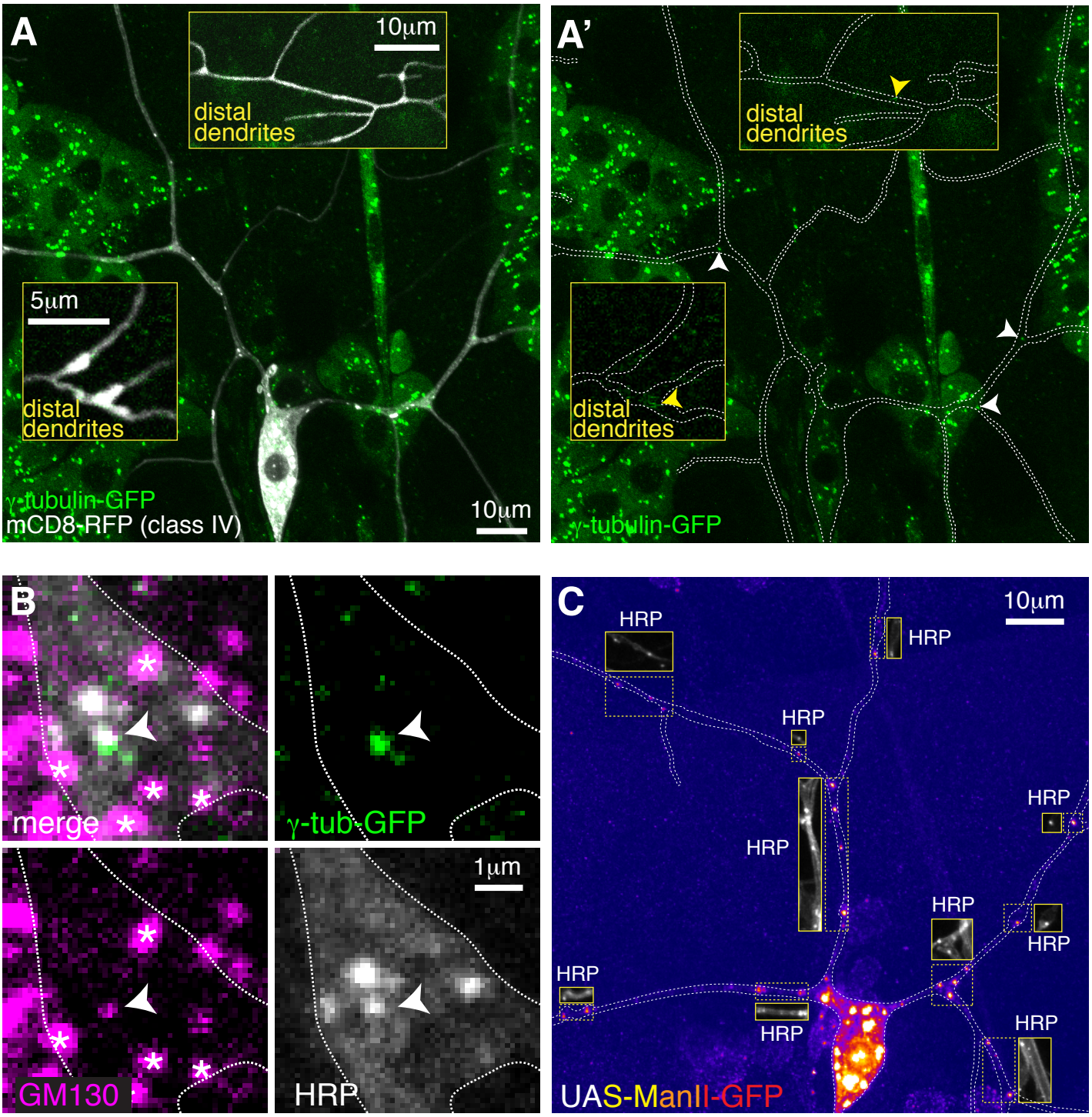
A
10μm
distal
dendrites
5μm
distal
dendrites
γ-tubulin-GFP
mCD8-RFP (class IV)
10μm
A'
distal
dendrites
distal
dendrites
γ-tubulin-GFP
B
merge
γ-tub-GFP
GM130
1μm
HRP
C
10μm
HRP
UAS-ManII-GFP

Figure 3

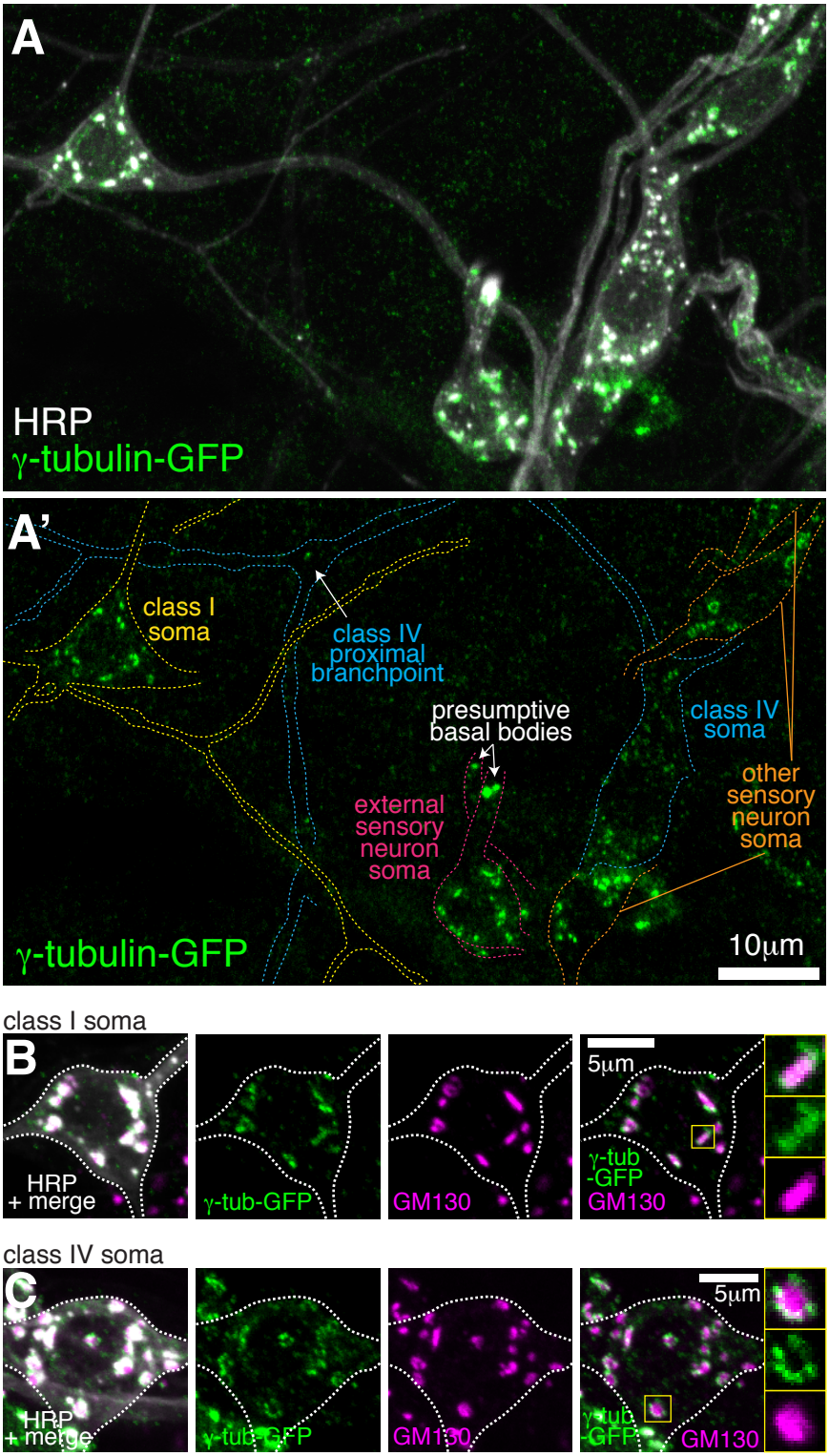
A
HRP
γ-tubulin-GFP
A'
class I
soma
class IV
proximal
branchpoint
presumptive
basal bodies
class IV
soma
other
sensory
neuron
soma
external
sensory
neuron
soma
γ-tubulin-GFP
10μm
class I soma
B
HRP
+ merge
γ-tub-GFP
GM130
5μm
γ-tub
-GFP
GM130
class IV soma
C
HRP
+ merge
γ-tub-GFP
GM130
5μm
γ-tub
-GFP
GM130

Figure 4

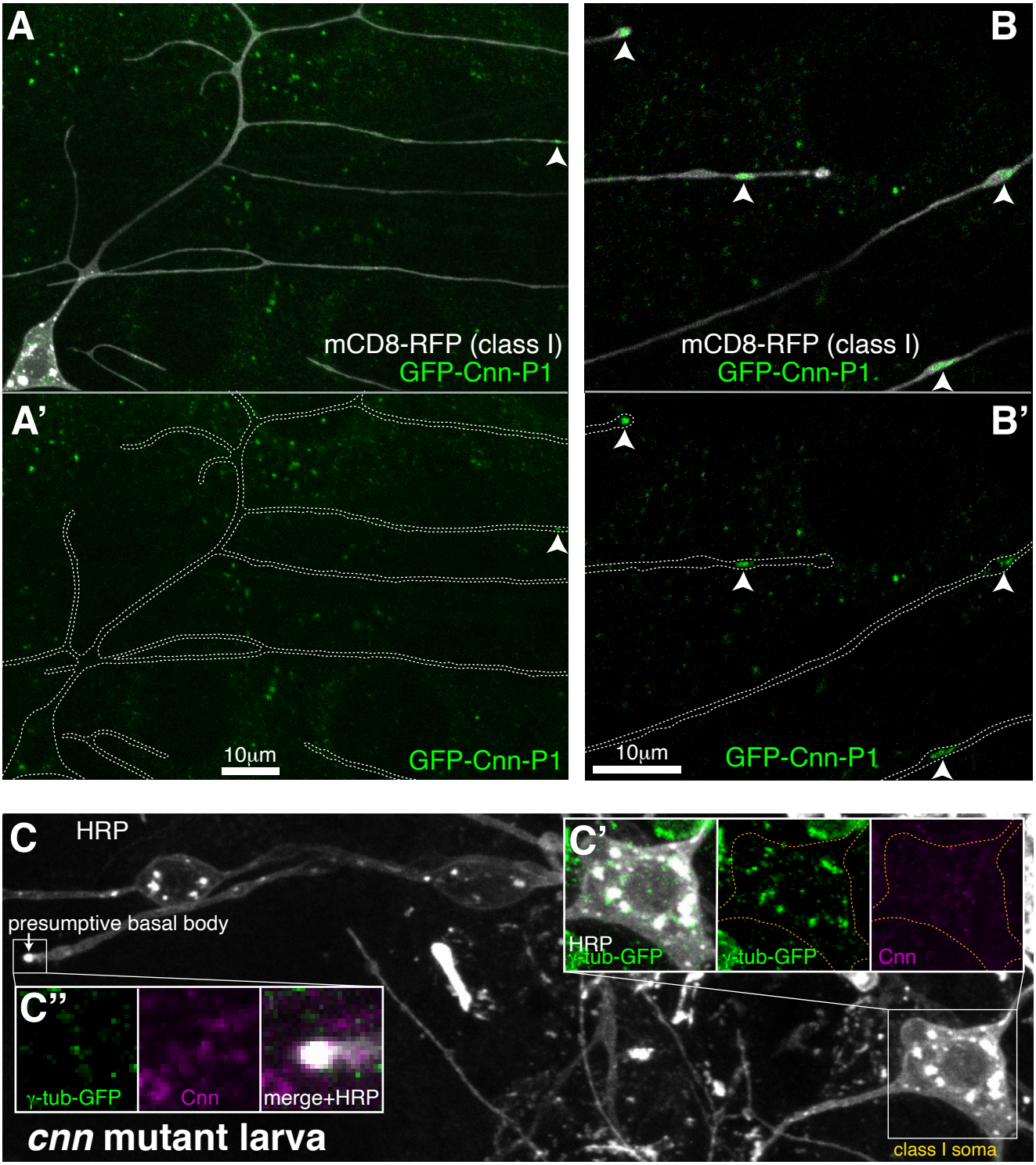
A
mCD8-RFP (class I)
GFP-Cnn-P1
B
mCD8-RFP (class I)
GFP-Cnn-P1
A'
10μm
GFP-Cnn-P1
B'
10μm
GFP-Cnn-P1
C
HRP
presumptive basal body
C'
HRP
γ-tub-GFP
γ-tub-GFP
Cnn
C''
γ-tub-GFP
Cnn
merge+HRP
cnn mutant larva
class I soma

Figure 5

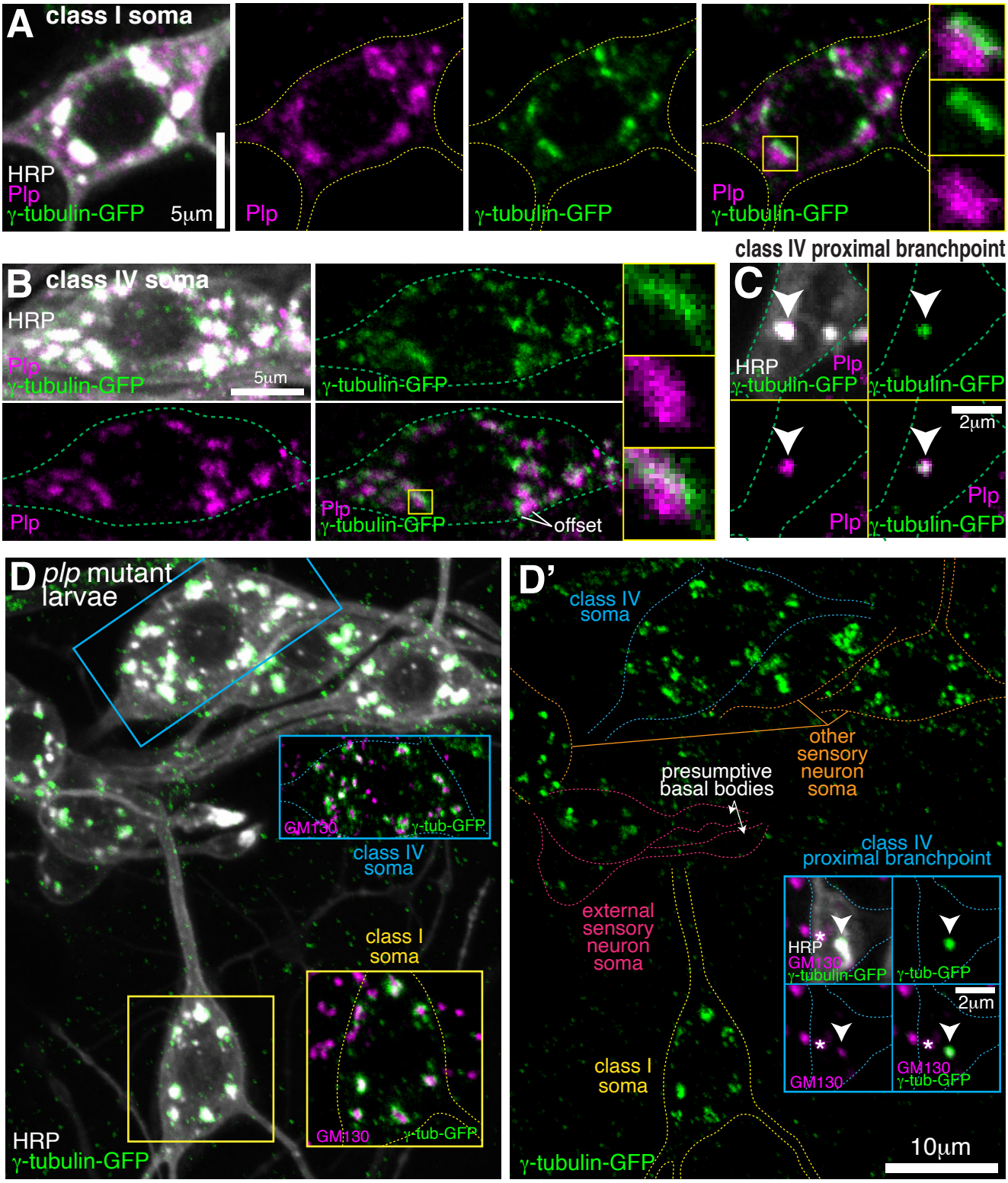
A
class I soma
HRP
Plp
γ-tubulin-GFP
5μm
Plp
γ-tubulin-GFP
Plp
γ-tubulin-GFP
B
class IV soma
HRP
Plp
γ-tubulin-GFP
5μm
γ-tubulin-GFP
Plp
Plp
γ-tubulin-GFP
offset
class IV proximal branchpoint
C
HRP
Plp
γ-tubulin-GFP
γ-tubulin-GFP
2μm
Plp
Plp
γ-tubulin-GFP
D
plp mutant larvae
GM130
γ-tub-GFP
class IV soma
class I soma
HRP
γ-tubulin-GFP
GM130
γ-tub-GFP
D'
class IV soma
other sensory neuron soma
presumptive basal bodies
class IV proximal branchpoint
external sensory neuron soma
HRP
GM130
γ-tubulin-GFP
γ-tub-GFP
2μm
GM130
GM130
γ-tub-GFP
class I soma
γ-tubulin-GFP
10μm

Figure 6

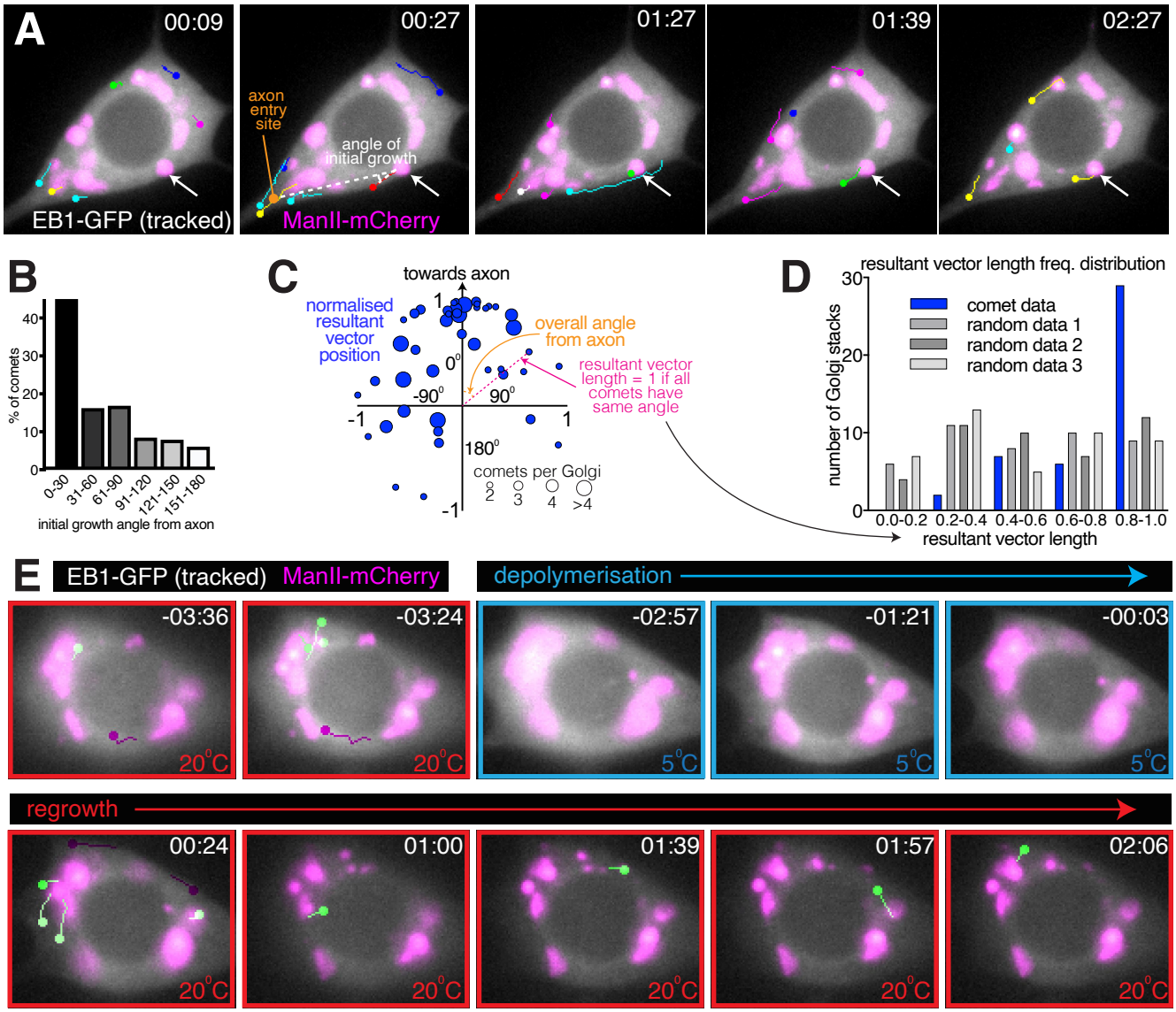
A
00:09
00:27
01:27
01:39
02:27
axon entry site
angle of initial growth
EB1-GFP (tracked)
ManII-mCherry
B
% of comets
initial growth angle from axon
0-30
31-60
61-90
91-120
121-150
151-180
C
towards axon
normalised resultant vector position
overall angle from axon
resultant vector length = 1 if all comets have same angle
comets per Golgi
D
resultant vector length freq. distribution
number of Golgi stacks
comet data
random data 1
random data 2
random data 3
resultant vector length
0.0-0.2
0.2-0.4
0.4-0.6
0.6-0.8
0.8-1.0
E
EB1-GFP (tracked)
ManII-mCherry
depolymerisation
-03:36
-03:24
-02:57
-01:21
-00:03
20°C
5°C
regrowth
00:24
01:00
01:39
01:57
02:06

Figure 7

control cells

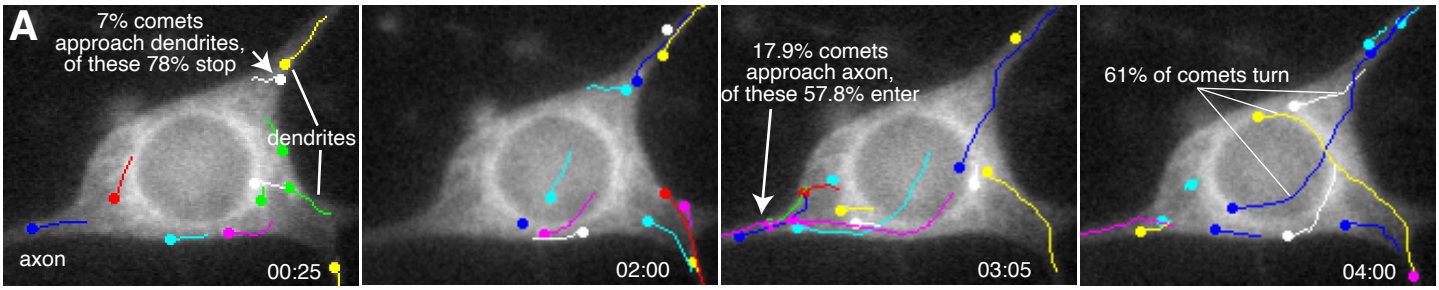

Kap3 (Kinesin-2) RNAi

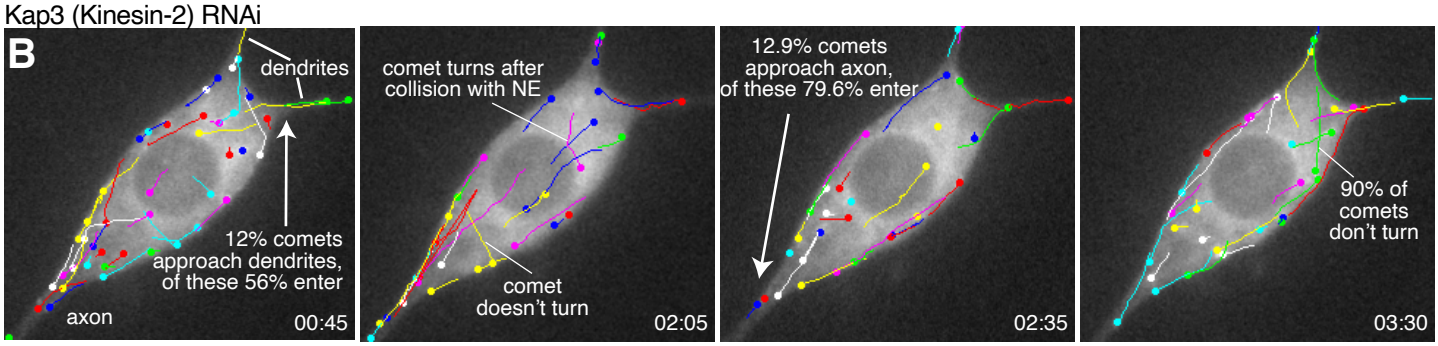

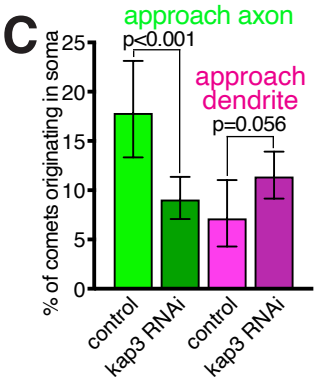

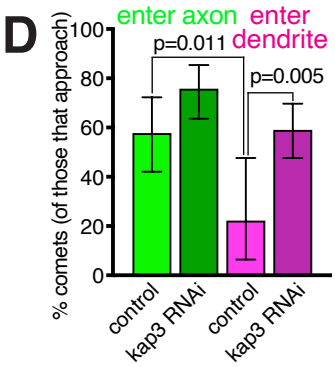

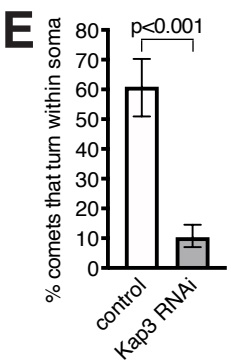

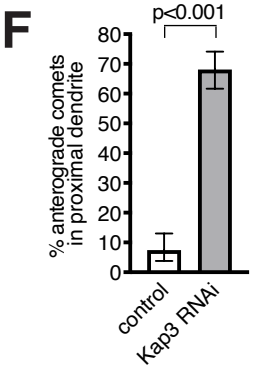

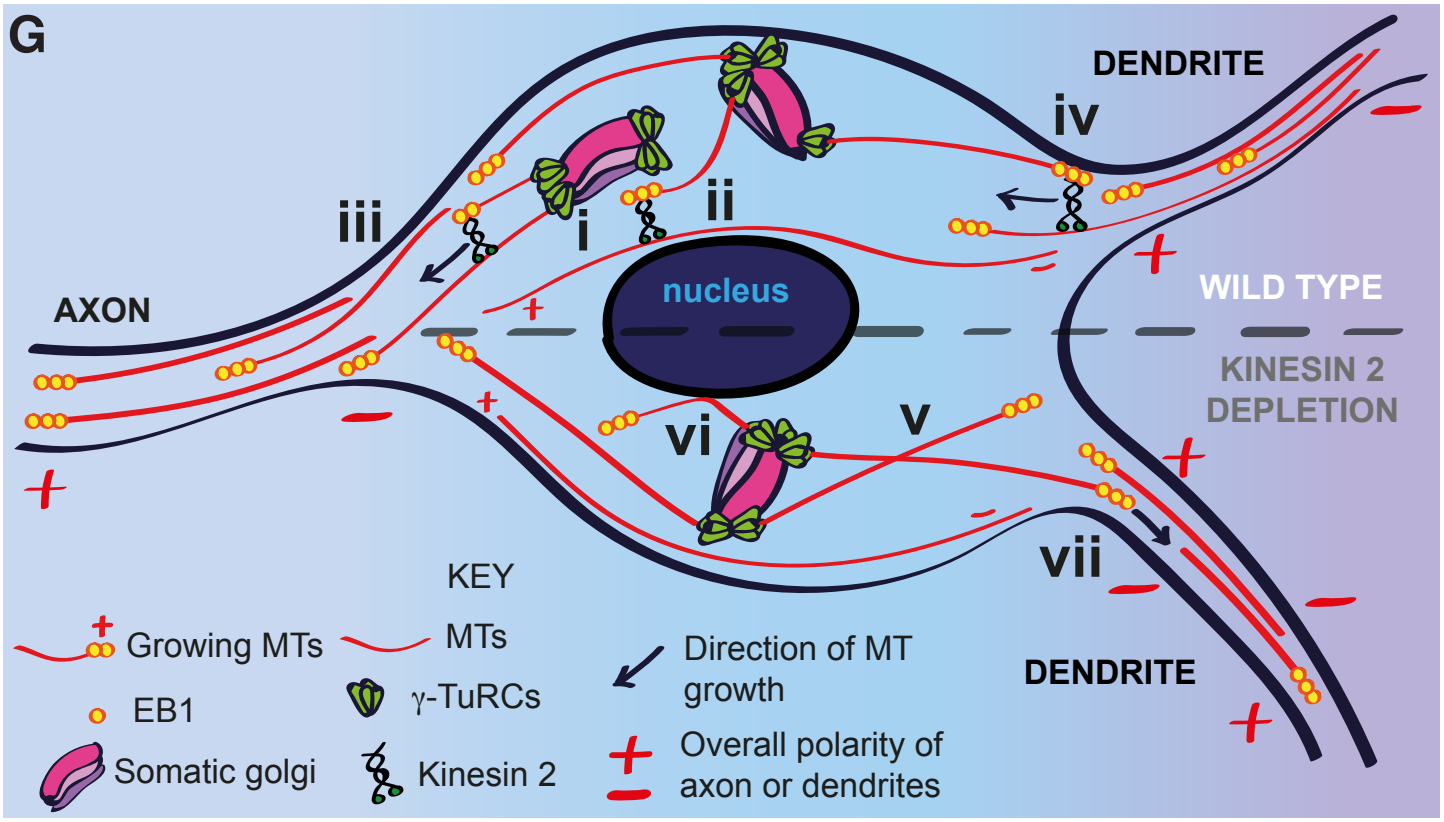

Figure S1

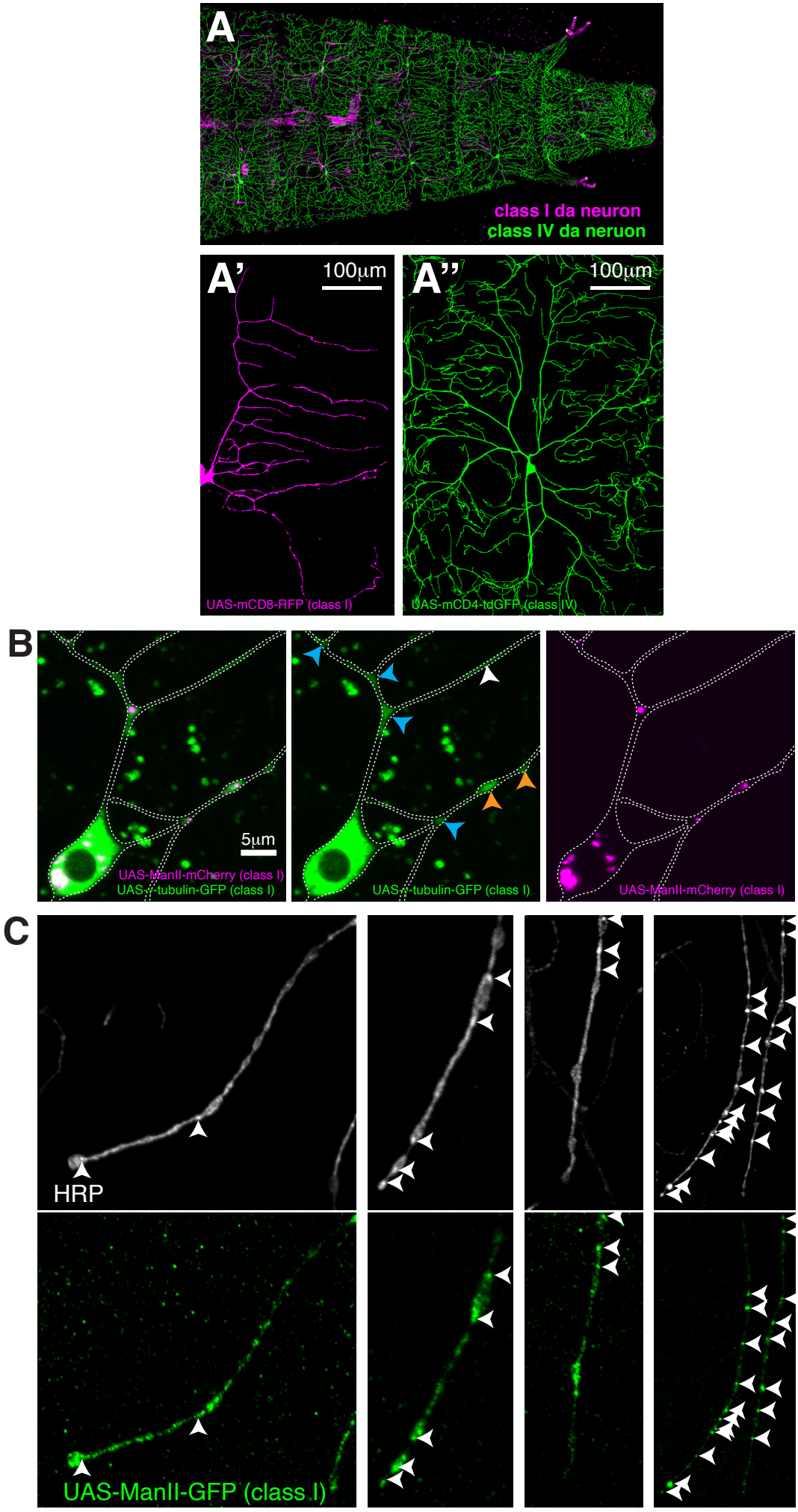
A
class I da neuron
class IV da neruon
A'
100μm
UAS-mCD8-RFP (class I)
A''
100μm
UAS-mCD4-tdGFP (class IV)
B
5μm
UAS-ManII-mCherry (class I)
UAS-γ-tubulin-GFP (class I)
UAS-γ-tubulin-GFP (class I)
UAS-ManII-mCherry (class I)
C
HRP
UAS-ManII-GFP (class I)

Figure S2

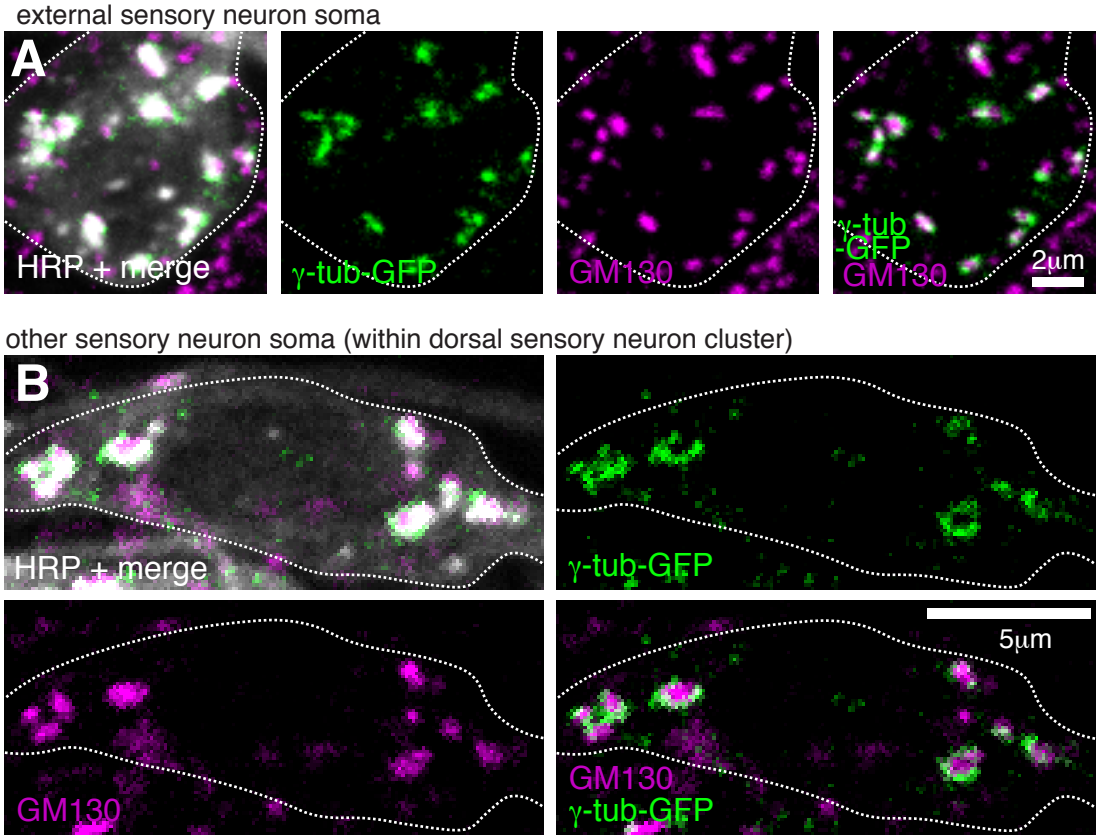
external sensory neuron soma
A
HRP + merge
γ-tub-GFP
GM130
γ-tub
-GFP
GM130
2μm
other sensory neuron soma (within dorsal sensory neuron cluster)
B
HRP + merge
γ-tub-GFP
GM130
5μm
GM130
γ-tub-GFP

Figure S3

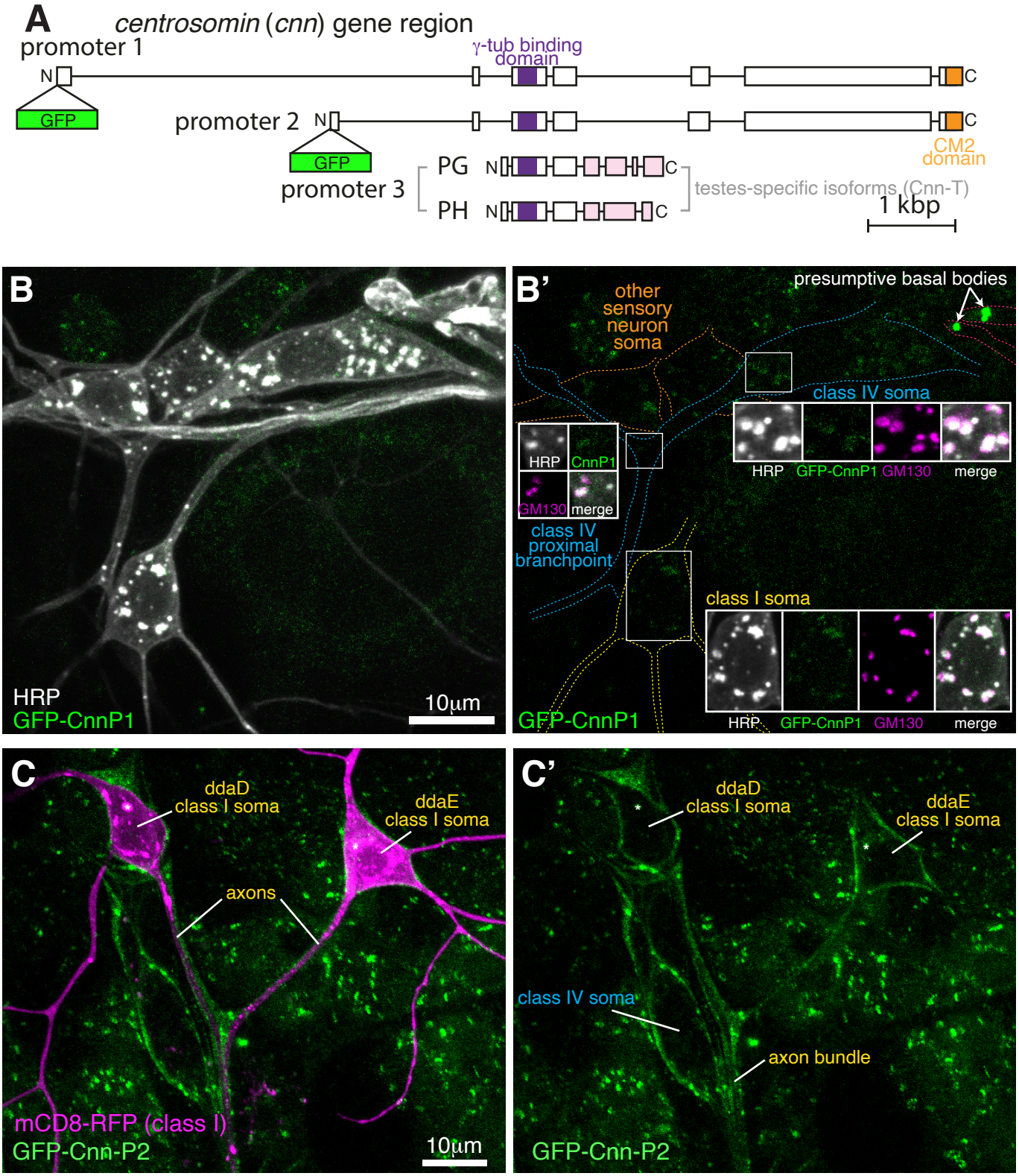
A
centrosomin (cnn) gene region
promoter 1
γ-tub binding domain
N
C
GFP
promoter 2
N
C
GFP
CM2 domain
promoter 3
PG
N
C
PH
N
C
testes-specific isoforms (Cnn-T)
1 kbp
B
HRP
GFP-CnnP1
10μm
B'
other sensory neuron soma
presumptive basal bodies
class IV soma
HRP
GFP-CnnP1
GM130
merge
HRP
CnnP1
GM130
merge
class IV proximal branchpoint
class I soma
HRP
GFP-CnnP1
GM130
merge
GFP-CnnP1
C
ddaD class I soma
ddaE class I soma
axons
mCD8-RFP (class I)
GFP-Cnn-P2
10μm
C'
ddaD class I soma
ddaE class I soma
class IV soma
axon bundle
GFP-Cnn-P2

Figure S4

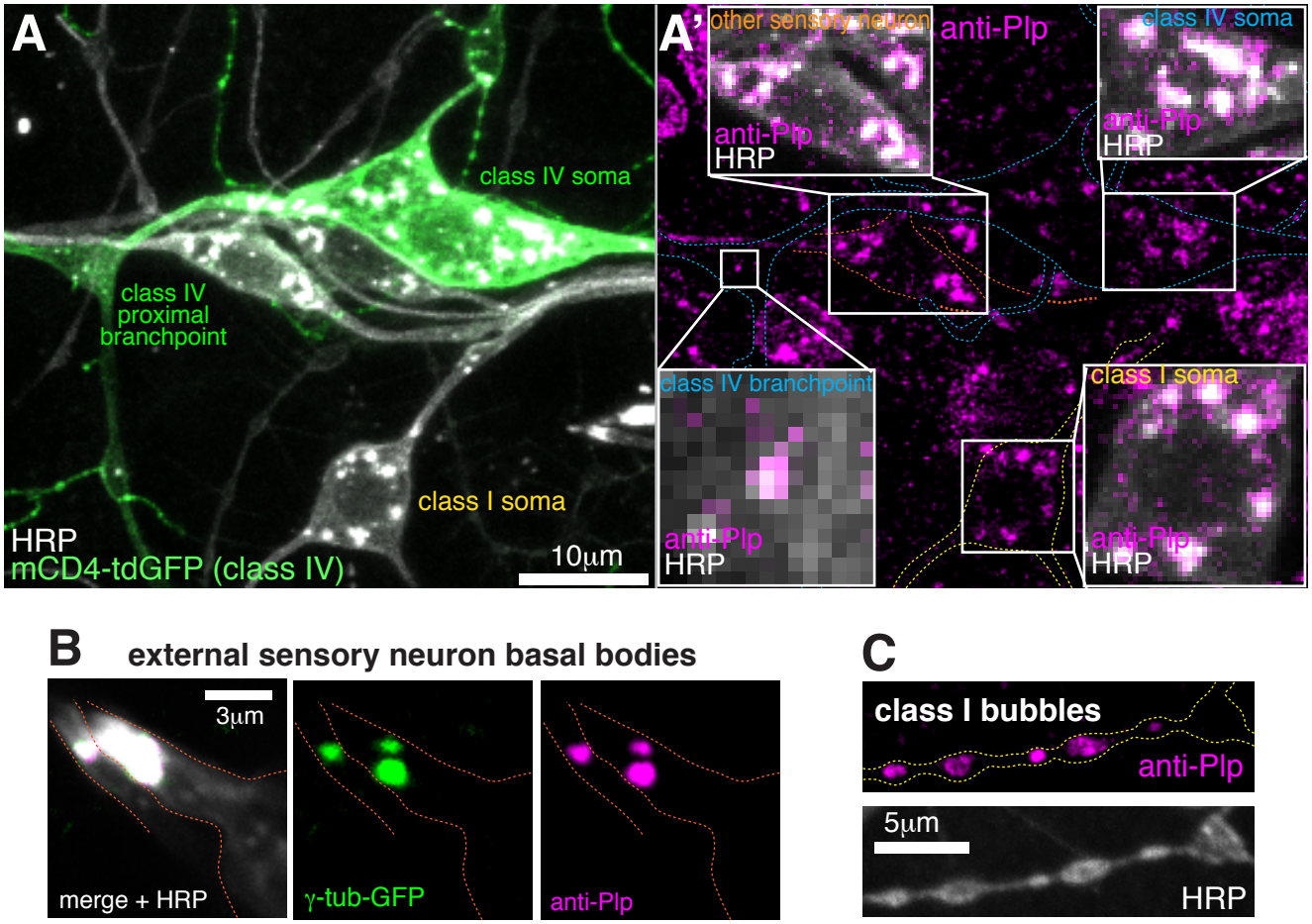
A
class IV soma
class IV
proximal
branchpoint
class I soma
HRP
mCD4-tdGFP (class IV)
10μm
A'
other sensory neuron
anti-Plp
class IV soma
anti-Plp
HRP
anti-Plp
HRP
class IV branchpoint
class I soma
anti-Plp
HRP
anti-Plp
HRP
B
external sensory neuron basal bodies
3μm
merge + HRP
γ-tub-GFP
anti-Plp
C
class I bubbles
anti-Plp
5μm
HRP